INSTITUTE OF PHYSICS PUBLISHING NONLINEARITY

Nonlinearity **19** (2006) 1875–1906 doi:10.1088/0951-7715/19/8/007

Multi-parametric bifurcations in a piecewise–linear discontinuous map

Viktor Avrutin[1], **Michael Schanz**[1] **and Soumitro Banerjee**[2]

[1] Institute of Parallel and Distributed Systems (IPVS), University of Stuttgart, Universitätstrasse 38, D-70569 Stuttgart, Germany
[2] Department of Electrical Engineering, Indian Institute of Technology, Kharagpur-721302, India

E-mail: viktor.avrutin@informatik.uni-stuttgart.de, michael.schanz@informatik.uni-stuttgart.de and soumitro@ee.iitkgp.ernet.in

Received 16 January 2006
Published 12 July 2006
Online at stacks.iop.org/Non/19/1875

Recommended by B Eckhardt

Abstract

In this paper a one-dimensional piecewise linear map with discontinuous system function is investigated. This map actually represents the normal form of the discrete-time representation of many practical systems in the neighbourhood of the point of discontinuity. In the 3D parameter space of this system we detect an infinite number of co-dimension one bifurcation planes, which meet along an infinite number of co-dimension two bifurcation curves. Furthermore, these curves meet at a few co-dimension three bifurcation points. Therefore, the investigation of the complete structure of the 3D parameter space can be reduced to the investigation of these co-dimension three bifurcations, which turn out to be of a generic type. Tracking the influence of these bifurcations, we explain a broad spectrum of bifurcation scenarios (like period increment and period adding) which are observed under variation of one control parameter. Additionally, the bifurcation structures which are induced by so-called big bang bifurcations and can be observed by variation of two control parameters can be explained.

PACS numbers: 02.30.Oz, 05.45.−a, 05.45.Ac

1. Introduction

In recent times the dynamics of piecewise smooth maps have received significant research attention [1–3] because a large number of systems of practical interest are modelled by such maps. This includes power electronic circuits [4], systems involving relays [5], mechanical systems with impacts [6, 7] and stick–slip oscillations [8], cardiac dynamics [9], walking robots [10], etc. Most of the efforts in developing the theory for border collision bifurcations have concentrated on piecewise smooth but continuous maps [1–3].

In contrast, discontinuous maps have received far less research attention even though many practical dynamical systems have been shown to be modelled by piecewise smooth maps with discontinuity at the boundary. Such maps occur in situations where there is a borderline in the Poincaré section such that two arbitrarily close points on the two sides of the border land far apart at the next observation instant. It has been shown that such a situation occurs in sigma–delta modulators [11], Colpitts oscillators [12], dc-dc converters [13] and many other electronic circuits [14]. To study the bifurcations occurring when a fixed point hits the discontinuity boundary, in [15] the piecewise linear normal form

$$\tilde{x}_{n+1} = \begin{cases} a\tilde{x}_n + \tilde{\mu} & \text{for} \quad \tilde{x}_n < 0 \\ b\tilde{x}_n + \tilde{\mu} + l & \text{for} \quad \tilde{x}_n > 0 \end{cases} \tag{1}$$

is considered and the bifurcation structures observed when one parameter ($\tilde{\mu}$) is varied are explored. This work provided the ground for analysing the unexpected sudden transitions in dynamical behaviour that cannot be explained using the well-developed theory for smooth maps as well as that for non-smooth but continuous maps. While this work has helped in understanding the bifurcations observed in practical systems [13], it raised some further questions. For example, it was shown that under certain conditions, orbits of progressively higher periodicities *in arithmetic progression* appear as a parameter are varied. In some cases the range of existence of subsequent orbits overlaps, resulting in parameter ranges with coexisting attractors. In other cases there are higher periodic or chaotic orbits sandwiched between the ranges of occurrence of consecutive periodic orbits in that progression. The questions arising are the following. What organizes such bifurcation sequences? Do such sequences continue *ad infinitum* or do they truncate after some periodicity? When does chaos occur?

In this paper we probe these questions and show that the answers can be obtained only when we take a look at the global character of the parameter space rather than by varying one parameter at a time. For this purpose we consider the map

$$\tilde{x}_{n+1} = \begin{cases} f_l(x_n) = ax_n + \mu & \text{for } x_n < 0, \\ f_r(x_n) = bx_n + \mu + 1 & \text{for } x_n > 0, \end{cases} \tag{2}$$

which is equivalent to system (2) for any $l > 0$. Hereby the variable x and the parameter μ have been rescaled using the relations $x = \tilde{x}/l$ and $\mu = \tilde{\mu}/l$, to bring the number of parameters down to three. Due to this equivalence all the bifurcation phenomena observable in both systems are identical. Note that the earlier work [15] considered both positive and negative values of the discontinuity, while for the present paper we take up only the case of the positive discontinuity to probe the specific questions considered in this paper.

Recall that the study of bifurcation phenomena with a variation of more than one parameter is not new, and the so-called co-dimension-2 bifurcations—which require the variation of more than one parameter for a complete description—have been reported in many systems. These bifurcations are discussed in the early works [16–21] and were intensively studied for instance in [22–26], and it is generally recognized that co-dimension-2 bifurcations are very important dynamical phenomena. In this paper we show that there can be a special and very interesting situation where *an infinity* of bifurcation curves meet at a point in the parameter space, and thus an infinite number of bifurcations occur as a parameter is varied through that point. We show that this special class of multi-parametric bifurcation organizes the structure of the bifurcation diagram in the discontinuous map.

The paper is organized as follows. In sections 2 and 3 we clearly state the notation and technical meaning of the terms we use throughout this paper. In section 4 we specify the region of the parameter space of system (2) under consideration. In section 5 we first explore the

character of the slice of the $a \times b \times \mu$ parameter space through the plane $a = 0$. In section 6 we explore the general case of nonzero values of a. In section 7 we show that in this system there can also be 3-parametric (co-dimension-3) bifurcation which organizes the dynamics in an extended region of the parameter space. The implications of results thus obtained are illustrated with two examples in section 8, after which we conclude.

2. Notations

For the investigation of periodic orbits, we will use one of the standard symbolic codings for 1D maps (the so-called $\mathcal{L}/\mathcal{R}$ dynamics, [27], see also [28]). For a point $x < 0$ we use the symbol $\mathcal{L}$ and for a point $x > 0$ the symbol $\mathcal{R}$. As usual, for a periodic orbit we write only the sequence corresponding to one period. For periodic orbits, we use sequences starting with the symbol $\mathcal{L}$ without loss of generality, since the symbolic sequences are shift-invariant. This is always possible because it can be easily shown that each periodic orbit in system (2) contains points from both regions $x < 0$ and $x > 0$. Additionally, a periodic orbit corresponding to symbolic sequence σ is denoted as O_σ. The area in parameter space where O_σ exists is denoted as $\mathcal{P}_\sigma$. The sequence σ is admissible for system (2), iff $\mathcal{P}_\sigma \neq \emptyset$.

3. Definitions

3.1. Domain of a bifurcation and multi-parametric bifurcations

Let us firstly summarize the nomenclature we use in this paper. Most of the terms we need are related to the concept of bifurcations in a multi-dimensional parameter space. As the *domain* of a bifurcation we denote the set of parameter values for which this bifurcation occurs. Sometimes domains of a bifurcation are called the bifurcation sets. Typically, a bifurcation's domain represents an $(n-1)$-dimensional subspace of the n-dimensional parameter space. In this case, the bifurcation is called *one-parametric*, often denoted also as *co-dimension one* bifurcation [22]. Particularly, in one-dimensional parameter spaces, there exist only one-parametric bifurcations and their domains are given by singular points (usually called bifurcation points). Obviously, in this case there are exactly two different asymptotic dynamics in the vicinity of the bifurcation point. In 2D parameter spaces the domains of one-parametric bifurcations are represented by curves, in 3D parameter spaces by surfaces and so on. Most of the well-known bifurcations, like transcritical, Hopf, pitchfork, flip, etc belong to this class.

However, in some cases the dimension of the bifurcation's domain is less than $n-1$. We denote such bifurcation as *multi-parametric* or as bifurcations with *higher co-dimension*. More precisely, if the domain of a bifurcation has the dimension m, then the bifurcation is $(n-m)$-parametric or has the co-dimension $(n-m)$. Obviously, such bifurcations can be observed only by investigation of n-dimensional parameter spaces with $n \geqslant 2$. It is well known that the co-dimension of a bifurcation is the minimal dimension of the parameter space required for an adequate description of this bifurcation.

Upto now, most of the known results were related to the case $n = 2$. In this case, the domains of one-parametric bifurcations are given by curves, and two-parametric bifurcations occur at points where one-parametric bifurcation curves intersect each other. An example of this phenomenon is the Hopf–Hopf bifurcation, which represents the intersection of two Hopf bifurcation curves. One can say that the Hopf–Hopf bifurcation is induced by two Hopf bifurcations occurring at the same point in the parameter space. Similarly, there can be two saddle-node bifurcations occurring at the same point in the parameter space.

In piecewise–smooth dynamical systems multi-parametric bifurcations are often induced by border-collision bifurcations.

3.2. Big bang bifurcations and characteristic 1D scenarios

A special type of two-parametric (or co-dimension-2) bifurcation is given by the case where, at some point in the parameter space, an infinite number of bifurcation curves intersect. In [29] it was proposed that these specific bifurcations be denoted as *big bang bifurcations*. The big bang bifurcations occurring in piecewise-smooth dynamical systems are typically induced by border-collision bifurcations [30]. However, these bifurcations may be induced by other bifurcations as well, for instance by flip bifurcations [31].

Typically, in the vicinity of the big bang bifurcation point, there exists an infinite number of different asymptotic dynamics. However, this property is neither necessary nor sufficient. On the one hand, an infinite number of bifurcation curves may monotonically converge to a point without crossing each other and without crossing that point. On the other hand, an infinite number of bifurcation curves do not imply an infinite number of asymptotic dynamics in the areas bounded by these curves. This is possible, because at one bifurcation curve the dynamics may switch from one type to another, then, at the next bifurcation curve, it may switch back to the first and so on. An example of a map which demonstrates this phenomenon can be found in [30].

Remarkably, the used definition of the big bang bifurcation does not specify what kind of bifurcation curves intersect at the bifurcation point and consequently, what kind of asymptotic dynamics exist in the vicinity of this point. In order to classify the big bang bifurcation more precisely, in [32] it is suggested to consider the one-parametric bifurcation scenario taking place along the border of an infinitely small convex open neighbourhood of the bifurcation point.

Typical bifurcation scenarios observed in the system under consideration, formed by repeated occurrence of border-collision bifurcations, can be classified into three possible scenarios. These are *period increment with coexistence of attractors, pure period increment* and *period adding* scenarios. In all three cases, there exists a sequence of periodic attractors, whose periods form an arithmetical series $p_n = p_0 + n\Delta p$ with a starting period p_0 and an increment value Δp. Let us denote as η_n the parameter value at which the attractor with period p_n is created and as $\bar{\eta}_n$ the value at which it is destroyed. Without any loss of generality, we can assume $\eta_n < \bar{\eta}_n$. η_{n+1} and $\bar{\eta}_{n+1}$ are the corresponding parameter values for the next periodic orbit in that sequence. Then, the common property of all three bifurcation scenarios mentioned above is given by $\eta_n < \eta_{n+1}$ and $\bar{\eta}_n < \bar{\eta}_{n+1}$, whereas the difference between the scenarios concerns the location of the values $\bar{\eta}_n$ and η_{n+1} with respect to each other. In particular, the scenarios mentioned above correspond to the cases $\bar{\eta}_n > \eta_{n+1}$, $\bar{\eta}_n = \eta_{n+1}$ and $\bar{\eta}_n < \eta_{n+1}$. In the case $\bar{\eta}_n > \eta_{n+1}$ the sequence of periods $p_n = p_0 + n\Delta p$ is caused by a sequence of pairs $(\eta_{n+1}, \bar{\eta}_n)$ of border-collision bifurcations. After the first bifurcation within the nth pair, i.e. after η_{n+1}, the attractor with period p_{n+1} emerges, but the attractor with period p_n continues to exist. Then, both attractors coexist between parameter values η_{n+1} and $\bar{\eta}_n$. At $\bar{\eta}_n$, the attractor with period n is destroyed. We denote this scenario as 'period increment with coexistence of attractors'. If such a bifurcation sequence is observed in the vicinity of a big bang bifurcation point, then this point is called a 'period increment big bang bifurcation with coexistence of attractors'.

In the case $\bar{\eta}_n = \eta_{n+1}$ both bifurcations occur at the same parameter value, so that the sequence of periods $p_n = p_0 + n\Delta p$ is caused by a sequence of double border-collision bifurcations. At the nth bifurcation, the attractor with period p_n is destroyed and the attractor

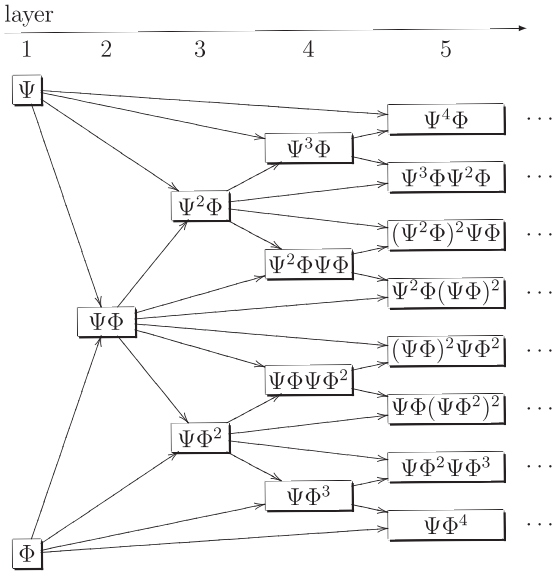

Figure 1. First layers of the infinite adding scheme generating periods occurring in the period adding scenario.

with period p_{n+1} simultaneously emerges. We denote this scenario as 'pure period increment' and the corresponding big bang bifurcation point as pure period increment big bang bifurcation or simply period increment big bang bifurcation.

The last case $\bar{\eta}_n < \eta_{n+1}$ is more complex. In this case between both bifurcations there is a gap, where the attractor with period p_n has already been destroyed and the attractor with period p_{n+1} has not yet emerged. In this parameter interval we observe higher-periodic attractors, whose periods can be calculated based on p_n and p_{n+1} using the infinite adding scheme for symbolic sequences [30]. The first layers of this scheme are shown in figure 1. The scheme can be continued layer-wise *ad infinitum* according to the following simple rule: a symbolic sequence in the mth layer of the period adding scheme is constructed via concatenation of a sequence from the $(m-1)$th layer with the corresponding direct successor of this sequence. Note that this infinite sequence adding scheme represents a natural extension of the well-known Farey trees [33] for the space of symbolic sequences.

Concerning the period adding scenario, let Ψ be the symbolic sequence corresponding to the attractor with period p_n and Φ the one corresponding to the attractor with period p_{n+1}. Remarkably, there exists a bijective topology-preserving mapping between the parameter space and the space of admissible symbolic sequences generated within the infinite adding scheme described above. Therefore we state that, for instance between periods p_n and p_{n+1}, there exists the period $p_n + p_{n+1}$ (corresponding to the symbolic sequence $\Psi\Phi$), between periods $p_n + p_{n+1}$ and p_{n+1} there exists the period $p_n + 2p_{n+1}$ (corresponding to the symbolic sequence $\Psi\Phi^2$) and so on. We denote this bifurcation scenario as period adding, and the corresponding big bang bifurcation is denoted as period adding big bang bifurcation.

3.3. Influence areas

Additionally, we use in this work the concept of the *influence area* of a bifurcation. We define this area as the contiguous region around a bifurcation point, where the parameter setting leads

to attractors which are topologically equivalent to the attractors existing in the vicinity of the bifurcation point. When dealing with 1D parameter spaces, this means simply the parameter interval between the previous and the next bifurcation.

In higher-dimensional parameter spaces, however, this concept becomes more interesting, because the influence area of a single multi-parametric bifurcation may cover large parts of the parameter space. This fact represents one of the main practical reasons for investigating multi-parametric bifurcations. Determining the type of a multi-parametric bifurcation, i.e. discovering the structure of its vicinity, one is often able to predict the behaviour of the investigated system in a large area of the complete multi-dimensional parameter space.

4. Parameter space region under consideration

In order to specify the area in the 3D parameter space, which we will investigate in detail in the following, let us first summarize some basic results related to the dynamic behaviour of system (2). A straightforward calculation shows that this system possesses at most two fixed points, namely,

$$x^*_{\mathcal{L}} = \frac{\mu}{1-a}, \qquad x^*_{\mathcal{R}} = \frac{\mu+1}{1-b}. \tag{3}$$

Because $x^*_{\mathcal{L}}$ is calculated using the left partial function f_l, it exists iff $\mu/(1-a) < 0$. Similarly, $x^*_{\mathcal{R}}$ exists iff $(\mu+1)/(1-b) > 0$. Note, that if a fixed point collides with the border $x = 0$, it is destroyed via a border-collision bifurcation. Therefore the parameter planes $\mu = -1$ and $\mu = 0$ in the 3D parameter space represent planes of border-collision bifurcations. Because the parameters a and b represent the slopes of the partial functions f_l and f_r, the fixed point $x^*_{\mathcal{L}}$ is stable iff $|a| < 1$ and $x^*_{\mathcal{R}}$ is stable iff $|b| < 1$. If $|a| < 1$ and $|b| < 1$, two stable fixed points coexist if $\mu \in (-1, 0)$ and outside this range there is one stable fixed point. If $|a| > 1$ and $|b| > 1$ then no periodic orbit can be stable and the attractors can be either chaotic or the fixed points at $\pm\infty$.

In the present paper our point of interest is that part of parameter space where high-periodic orbits are possible. Therefore we exclude the above regions. Out of the remaining regions in the parameter space we concentrate on two cases:

$$\mathcal{P} = \{(a, b, \mu) \mid |a| < 1, b < -1, \mu \geqslant 0\}, \tag{4}$$

$$\mathcal{P}' = \{(a, b, \mu) \mid a < -1, |b| < 1, \mu \leqslant -1\}, \tag{5}$$

where high-periodic orbits can occur. A preliminary study of the bifurcation phenomena in these regions of the parameter space was reported in [15]. In this paper we make an in-depth investigation of the sequences of periodic orbits and demonstrate the occurrence of big bang bifurcations. Since the parameter space is three dimensional, for the sake of visualization we analyse $b \times \mu$ slices of the parameter space for specific values of a.

Note that the system function has the symmetry

$$f(a, b, \mu, x) = -f(b, a, -(\mu+1), -x) \tag{6}$$

and hence there is a one-to-one correspondence between the bifurcation structures in the regions $\mathcal{P}$ and $\mathcal{P}'$. This is why in the rest of the paper we concentrate only on the region $\mathcal{P}$.

5. Plane $b \times \mu$ for $a = 0$

5.1. Numerical observations

Let us start with the case $a = 0$. As shown in figures 2(*a*) and (*c*), under variation of the parameter b, system (2) demonstrates a typical period increment scenario with the increment

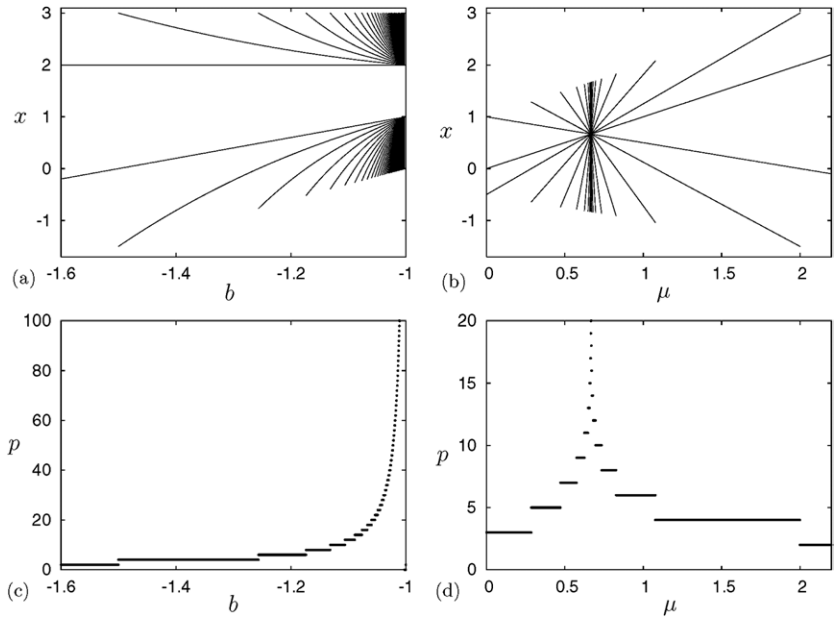

Figure 2. Bifurcation and period diagrams in the case $a = 0$ under variation of one control parameter. (a), (c) $\mu = 2$, b varied. (b), (d) $b = -1.5$, μ varied.

value $\Delta p = 2$. This scenario converges to the boundary $b = -1$ of the investigated area in the parameter space. The behaviour under the variation of the parameter μ is similar, however in this case two period increment scenarios converging to the same accumulation point $\mu_c = \frac{2}{3}$ can be observed (figures 2(b) and (d)). Remarkably, both scenarios have the same increment value $\Delta p = 2$, but different start values $p_0 = 2$ and $p_0 = 3$. Consequently, one of these scenarios (shown in the left part of figures 2(b) and (d)) is formed by attractors with even periods and the other one by attractors with odd periods.

5.2. Emergence of periodic orbits

In order to explain the results obtained numerically, let us consider the mechanism causing the periodic orbits of system (2) to occur. It can be easily shown that each periodic orbit of this system contains points lying in the left half-axis $x < 0$ as well as in the right half-axis $x > 0$. Hence, without loss of generality we can consider a start point $x_0 < 0$. Because the slope of the left partial function f_l is equal to zero, each $x_0 < 0$ is mapped to $x_1 = \mu > 0$ within one iteration step. After that the orbit performs some number n of iteration steps on the right and is finally mapped to a point $x_{n+1} < 0$. Due to $a = 0$, this point is mapped to x_1 and hence the orbit becomes periodic. For this reason only sequences $\mathcal{LR}^n$ are admissible in the case $a = 0$.

In order to calculate the existence area of $O_{\mathcal{LR}^n}$, we have to take into account the fact that the bifurcations leading to these orbits are border-collision bifurcations. For $O_{\mathcal{LR}^n}$ two such bifurcations are possible. The first occurs if the point x_0 collides with the border $x = 0$ from the left side. The second one occurs if the point x_{n-1} collides with the border $x = 0$ from the right. Hence, we calculate (in general, i.e. not only for $a = 0$)

the values

$$x_0 = -\frac{\left(b^{n+1}-1\right)\mu + (b^n - 1)}{(ab^n - 1)\,(b-1)}, \tag{7}$$

$$x_{n-1} = ab^{n-2}x_0 + \frac{(b^{n-1}-1)\mu + (b^{n-2}-1)}{b-1}. \tag{8}$$

From the conditions $x_0 = 0$ and $x_{n-1} = 0$ we obtain the parameter values corresponding to the border-collision bifurcations

$$\xi_{\mathcal{LR}^n}^{x_0,l} = \left\{(a,b,\mu)\;\middle|\; -1 < a < 1, b < -1, \mu = -\frac{b^n - 1}{b^{n+1}-1}\right\}, \tag{9}$$

$$\xi_{\mathcal{LR}^n}^{x_{n-1},r} = \left\{(a,b,\mu)\;\middle|\; -1 < a < 1, b < -1, \mu = -\frac{b^{n-2}(1-a) - 1 + ab^n}{b^{n-2}(b-a) - 1 + ab^n}\right\}. \tag{10}$$

The notation used here guarantees a unique description for border-collision bifurcations of periodic orbits for dynamical systems with one discontinuity point. It has the following meaning: the lower index determines which orbit undergoes the bifurcation, and the upper indices, which point of this orbit collides with the border from which side. As an example, $\xi_\sigma^{x_2,r}$ would denote the parameter values of the border-collision bifurcation which occurs if the second point of O_σ collides with the border $x = 0$ from the right side. Note, that $\xi_{\mathcal{LR}^n}^{x_0,l}$ and $\xi_{\mathcal{LR}^n}^{x_{n-1},r}$ represent bifurcation surfaces in the 3D parameter space $a \times b \times \mu$.

Let us remark additionally, that for the special case $a = 0$ the bifurcation curve $\xi_{\mathcal{LR}^n}^{x_0,l}|_{a=0}$ (i.e. the intersection of the bifurcation surface $\xi_{\mathcal{LR}^n}^{x_0,l}$ with the plane $a = 0$) is identical with the bifurcation curve $\xi_{\mathcal{LR}^{n+2}}^{x_{n+1},r}|_{a=0}$. Indeed, setting $a = 0$ and replacing n with $n+2$ in the right-hand side of equation (10), one obtains the right-hand side of equation (9). For this reason we observe in the case $a = 0$ a double border-collision bifurcation which causes one of the limit cycles to emerge and the other one to disappear at the same parameter value. In contrast to this, for $a \neq 0$ these two phenomena (emergence of one limit cycle and destruction of the other one) are independent of each other. Both phenomena are caused by border-collision bifurcations, but the bifurcations may occur at different parameter values.

Note, that in the case $a = 0$ all periodic orbits $O_{\mathcal{LR}^n}$ are stable within their complete existence area. Moreover, because the derivative of the system function at the point $x_0 < 0$ is equal to zero, all these orbits are super-stable, i.e. their Lyapunov exponent tends to $-\infty$.

5.3. Emergence of odd and even periods

In order to understand the structure of the parameter plane $b \times \mu$ for the case $a = 0$, one has to take into account the fact that the orbit $O_{\mathcal{LR}^n}$, once mapped onto the right half-axis, performs some kind of circulation around the unstable fixed point $x_{\mathcal{R}}^*$. This explains the period increment value $\Delta p = 2$ mentioned above, because each circulation consists of two points. One of these points lies between zero and $x_{\mathcal{R}}^*$ whereas the other one is located on the right side of $x_{\mathcal{R}}^*$. This circulation around $x_{\mathcal{R}}^*$ is finished at the point x_n with $f_r(x_n) < 0$. Due to the negative slope of the function f_r, this point lies always on the right side of $x_{\mathcal{R}}^*$. Therefore, there are three characteristic cases, depending on the position of the point $x_1 = \mu$ with respect to the fixed point $x_{\mathcal{R}}^*$ as follows.

Case $x_1 = \mu > x_{\mathcal{R}}^*$: in this case a periodic orbit performs a number m of rotations around $x_{\mathcal{R}}^*$, or, equivalently, an even number of steps until it is mapped onto $x_0 < 0$ (see figure 3(*a*)). These orbits correspond to admissible sequences $\mathcal{LR}^{2m+1}$.

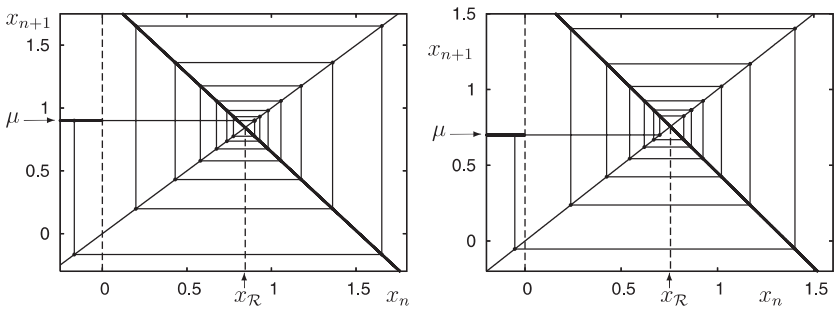

(a) $x_1 = \mu = 0.9 > x^*_{\mathcal{R}} \approx 0.8444$ (b) $x_1 = \mu = 0.7 < x^*_{\mathcal{R}} \approx 0.7556$

Figure 3. Periodical orbits $O_{\mathcal{LR}^{12}}$ and $O_{\mathcal{LR}^{13}}$ in the case $a = 0$, $b = -1.25$. As one can see, the period of the orbit is odd iff $\mu < x^*_{\mathcal{R}}$ and even iff $\mu > x^*_{\mathcal{R}}$.

Case $x_1 = \mu = x^*_{\mathcal{R}}$: in this case any point x_0 is mapped directly on to the fixed point. Therefore, the behaviour of system (2) is in this case somehow curious: although the fixed point $x^*_{\mathcal{R}}$ is locally unstable (since $|b| > 1$), it is globally stable as all orbits converge to this fixed point. Recall that the initial values leading to an unstable invariant set (for instance a fixed point) are usually denoted as atypical initial values. Hence, we state that in the case $\mu = x^*_{\mathcal{R}}$ each initial value is atypical.

Case $x_1 = \mu < x^*_{\mathcal{R}}$: in this case a periodic orbit performs an additional iteration step before it performs a number m of rotations around $x^*_{\mathcal{R}}$. Therefore, the complete number of iteration steps until the orbit is mapped onto $x_0 < 0$ is odd in this case (see figure 3(*b*)), and the corresponding admissible sequences are $\mathcal{LR}^{2m}$.

From equation (3) we obtain that the condition $\mu = x^*_{\mathcal{R}}$ is identical with $\mu = -1/b$. Therefore the situation described above for the case $\mu = x^*_{\mathcal{R}}$ occurs for the parameter values belonging to the bifurcation curve

$$\xi_\infty = \left\{ (a, b, \mu) \,\middle|\, a = 0, b < -1, \mu = -\frac{1}{b} \right\} = \lim_{n\to\infty} \xi^{x_0,l}_{\mathcal{LR}^n}\Big|_{a=0}. \tag{11}$$

This curve will play an important role for the explanation of the observed bifurcation structures (see sections 5.5 and 6.4).

5.4. Big bang bifurcations

As one can see from equation (9), the course of the curves $\xi^{x_0,l}_{\mathcal{LR}^n}|_{a=0}$ (and consequently of $\xi^{x_{n-1},r}_{\mathcal{LR}^n}|_{a=0}$, because for all n these curves are identical with $\xi^{x_0,l}_{\mathcal{LR}^{n-2}}|_{a=0}$) depends on whether the number n is even or odd. For $b \to -1$ the family of curves $\xi^{x_0,l}_{\mathcal{LR}^n}|_{a=0}$ with odd numbers n converge from the left side to the point

$$B^{\mathrm{I}}(a)|_{a=0} = \{a, b = -1, \mu \to \infty\}|_{a=0}, \tag{12}$$

whereas the family of curves $\xi^{x_0,l}_{\mathcal{LR}^n}|_{a=0}$ with even numbers n converge to the point

$$B^{\mathrm{II}}(a)|_{a=0} = \{a, b = -1, \mu = 0\}|_{a=0}. \tag{13}$$

In the limit case $b = -1$ the corresponding curves intersect at the points $B^{\mathrm{I}}(a)|_{a=0}$ and $B^{\mathrm{II}}(a)|_{a=0}$, so that these points represent the special class of two-parametric bifurcations which we have termed as big bang bifurcations. Recall, that the period of the asymptotic dynamic is increased by two at each of the curves $\xi^{x_0,l}_{\mathcal{LR}^n}|_{a=0}$. Therefore, the points $B^{\mathrm{I}}(a)|_{a=0}$ and $B^{\mathrm{II}}(a)|_{a=0}$

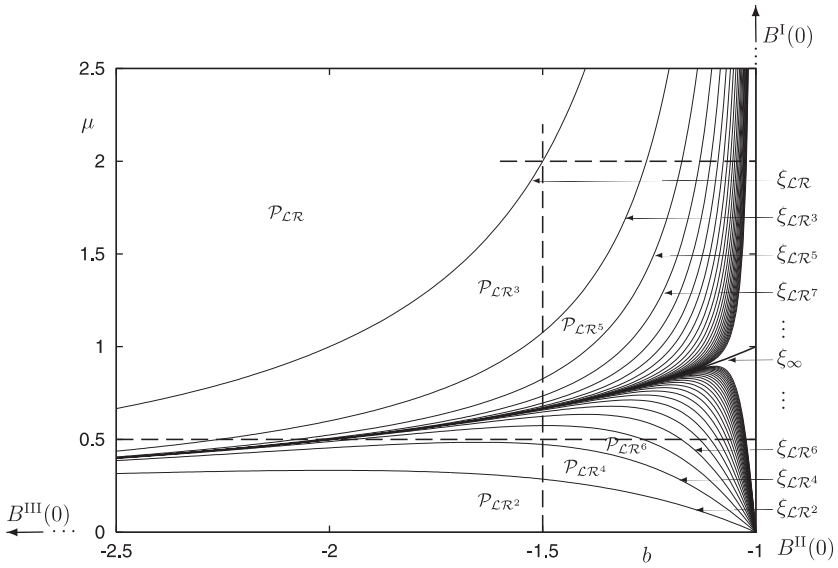

Figure 4. Analytically calculated structure of the plane $b \times \mu$ for $a = 0$. Shown are the curves ξ_n with $n = 1.50$ and the accumulation curve ξ_∞. The dashed lines $b = -1.5$ and $\mu = 2$ correspond to figure 2. The dashed line $\mu = 0.5$ corresponds to the example discussed in section 8.2.

(or, more simply, $B^{\mathrm{I}}(0)$ and $B^{\mathrm{II}}(0)$) represent pure period increment big bang bifurcations in the plane $b \times \mu$. Additionally, for all n (both odd and even) the bifurcation curves $\xi_{\mathcal{LR}^n}^{x_0,l}|_{a=0}$ converge to the point

$$B^{\mathrm{III}}(a) = \{a, b \to -\infty, \mu = 0\}. \tag{14}$$

Hence, in the plane $b \times \mu$ this point represents a big bang bifurcation as well. Note that the two points $B^{\mathrm{I}}(a)$ and $B^{\mathrm{III}}(a)$ can be shifted to finite values by a suitable transformation of the parameters. This also eliminates the problem regarding the mathematical correctness of the term 'infinite small vicinity of the point infinity'.

The type of big bang bifurcation occurring at the point $B^{\mathrm{III}}(0)$ does not fit exactly our definition of the period increment big bang bifurcation, because around the border of a vicinity of this point two period increment scenarios occur. However, this big bang bifurcation is closely related to the pure period increment big bang bifurcation. The bifurcation scenario along an infinite small vicinity of the point $B^{\mathrm{III}}(0)$ represents a double period increment scenario converging to the same accumulation point. As one can see from figure 4, this scenario is topologically equivalent to the one presented in figures 2(b) and (d).

We remark additionally, that period increment big bang bifurcations occur frequently pairwise (see for instance an example in [29]). This seems to be the natural way that the bifurcation lines originating from one of these bifurcations accumulate at the other one (this can be interpreted as some kind of interaction between the two involved period increment big bang bifurcations). In the case of system (2) for $a = 0$ we observe two period increment big bang bifurcations $B^{\mathrm{I}}(0)$ and $B^{\mathrm{II}}(0)$, both interacting in the described way with the big bang bifurcation $B^{\mathrm{III}}(0)$.

The phenomenon described above can be understood more easily considering the graph shown in figure 5. This graph (we call it the structural graph) represents the bifurcation structure of the 2D parameter plane $b \times \mu$ for the case $a = 0$. The vertices of the graph correspond to the two-parametric bifurcations in this plane. Two vertices are connected by an edge iff

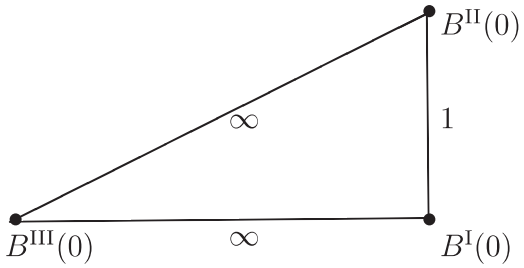

Figure 5. Schematic representation of the bifurcation structure of the plane $b \times \mu$ for $a = 0$.

there exists a bifurcation curve, which originates at one of the involved bifurcations and ends at the other one. The weight of an edge reflects the number of such curves. According to our definition, at a big bang bifurcation point an infinite number of bifurcation curves originate. Of course, all these curves may end at different bifurcation points, but the simplest case is obtained where all these curves are 'collected' by another big bang bifurcation. In this case all the bifurcation curves are represented in the structural graph by a single edge with the weight ∞. In the structural graph of system (2) for the plane $a = 0$, there exist two edges with weight ∞ between the big bang bifurcations $B^{\mathrm{I}}(0)$ and $B^{\mathrm{III}}(0)$ as well as between $B^{\mathrm{II}}(0)$ and $B^{\mathrm{III}}(0)$ (compare figure 4). The bifurcations $B^{\mathrm{I}}(0)$ and $B^{\mathrm{II}}(0)$ are connected by an edge with weight 1, which corresponds to the bifurcation where the fixed point $x^*_{\mathcal{R}}$ becomes unstable.

5.5. Influence areas

Figure 4 shows the analytically calculated structure of the plane $b \times \mu$ for the case $a = 0$. We state that in the case $a = 0$ that this area is completely influenced by the two big bang bifurcations at $B^{\mathrm{I}}(0)$ and $B^{\mathrm{II}}(0)$. This means that the existence area of any attractor of the investigated system starts in the case $a = 0$ at one of these points. In other words, the complete investigated area in the parameter space is covered by existence areas of attractors emerging at these bifurcations:

$$\Omega(B^{\mathrm{I}}(0))|_{a=0} = \bigcup_{n=0}^{\infty} \mathcal{P}_{\mathcal{LR}^{2n+1}} = \left\{(b, \mu) \mid \mu > -\frac{1}{b}\right\}, \tag{15}$$

$$\Omega(B^{\mathrm{II}}(0))|_{a=0} = \bigcup_{n=1}^{\infty} \mathcal{P}_{\mathcal{LR}^{2n}} = \left\{(b, \mu) \mid \mu < -\frac{1}{b}\right\} = \mathcal{P} \setminus \Omega(B^{\mathrm{I}}(0))|_{a=0}. \tag{16}$$

In relation to the used notation, recall that the influence areas $\Omega(B^{\mathrm{I}}(0))$ and $\Omega(B^{\mathrm{II}}(0))$ of the bifurcations occurring at $B^{\mathrm{I}}(0)$ and $B^{\mathrm{II}}(0)$ are 3D objects in the parameter space $a \times b \times \mu$. With $\Omega(B^{\mathrm{I}}(0))|_{a=0}$ and $\Omega(B^{\mathrm{II}}(0))|_{a=0}$ we denote the intersection areas of these 3D objects with the plane $a = 0$. Remarkably, the curve ξ_∞, which corresponds to the case $x^*_{\mathcal{R}} = \mu$, represents a border between the areas influenced by these two bifurcations and hence can be interpreted as some kind of 'separatrix' in the parameter space. Related to $B^{\mathrm{III}}(0)$, we state that the influence area of this bifurcation covers the complete area $\mathcal{P}$:

$$\Omega(B^{\mathrm{III}}(0))|_{a=0} = \Omega(B^{\mathrm{I}}(0))|_{a=0} \cup \Omega(B^{\mathrm{II}})(0)|_{a=0} = \mathcal{P}. \tag{17}$$

5.6. Numerical observations revisited

Now the results obtained numerically can be explained easily. The period increment scenario presented in figures 2(*a*) and (*c*) is observed under the variation of the parameter b for fixed value $\mu = 2$. As one can see, the investigated parameter intervals lie completely above the curve ξ_∞, i.e. within the area $\Omega(B^{\mathrm{I}}(0))|_{a=0}$ (see the horizontal line at $\mu = 2$ in figure 4). Consequently, the observed bifurcation scenario is formed by a sequence of periodic orbits $O_{\mathcal{LR}^{2n+1}}$. In contrast to this, fixing $b = -3/2$ and varying μ, one crosses the curve ξ_∞ (see the vertical line in figure 4). This leads to two period increment scenarios with a common accumulation point $\mu_c = 2/3$ as shown in figures 2(*b*) and (*d*). The left scenario (for $\mu < 2/3$) belongs to $\Omega(B^{\mathrm{II}}(0))|_{a=0}$. One can say that this scenario is caused by the period increment big bang bifurcation occurring at $B^{\mathrm{II}}(0)$, whereas the other one belongs to $\Omega(B^{\mathrm{I}}(0))|_{a=0}$.

6. Plane $b \times \mu$ for the case $a \neq 0$

As shown in the previous section, if the slope of the left partial function f_l is equal to zero, the investigated area in the parameter plane $b \times \mu$ is completely covered by areas $\mathcal{P}_{\mathcal{LR}^n}$. The next question arising in this context is how the structure of the parameter space is transformed, if the slope of the function f_l becomes non-zero.

6.1. Numerical observations

Let us firstly consider the case $a > 0$. In this case, investigating the behaviour of system (2) under the variation of one parameter, one observes a large number of different bifurcation scenarios. For instance, in figure 6 the behaviour is mainly caused by period adding phenomena. All attractors existing in the right part of these figures are periodic (figure 6(*c*)); the values of the Lyapunov exponent are negative (figure 6(*c*)) and show a structure typical of the period adding phenomenon.

In the left parts of figures 6(*a*)–(*c*) the behaviour becomes chaotic and one can observe one-band as well as multi-band attractors. Note that when looking only at the bifurcation diagram it is difficult to recognize the critical parameter value where the transition to chaos occurs. As one can see, the overall shape of the high-periodic attractors before and the chaotic attractors after this transition are similar. Remarkably, there are no periodic windows in this parameter range, i.e. the chaotic attractors existing below some critical value of b are robust. Note that this critical value of b depends on the parameters a and μ and can be calculated from equation (25) derived later. For the values $a = 0.2$, $\mu = 0.4$ used in figure 6 we obtain the critical value $b = -1.8$.

Another example of the behaviour observed for $a > 0$ is shown in figure 7. In this case we detect the orbits $O_{\mathcal{LR}}$, $O_{\mathcal{LR}^3}$, $O_{\mathcal{LR}^5}$ and $O_{\mathcal{LR}^7}$. The observed behaviour has some similarities with both period increment and period adding scenarios described above. On the one hand, we observe an arithmetical series of periods: 2, 4, 6, 8, similarly to the case of the period increment. However, the scenario is truncated: after the period 8 there are no further periods, but only a sequence of multi-band chaotic attractors. On the other hand, between each pair of periods there is some 'free space' (which means that the situation is similar to the case $\bar{\eta}_n < \eta_{n+1}$ discussed in section 3.2 for the period adding). However, between parameter intervals leading to corresponding periodic orbits there are intervals leading to chaotic behaviour and not to a periodic one, in contrast to the case of the period adding scenario.

For a negative value $a = -0.05$ we observe the complex scenario presented in figure 8. As one can see, this scenario begins as a typical period adding, followed by a parameter interval with chaotic dynamics and is continued as a period increment scenario with coexisting

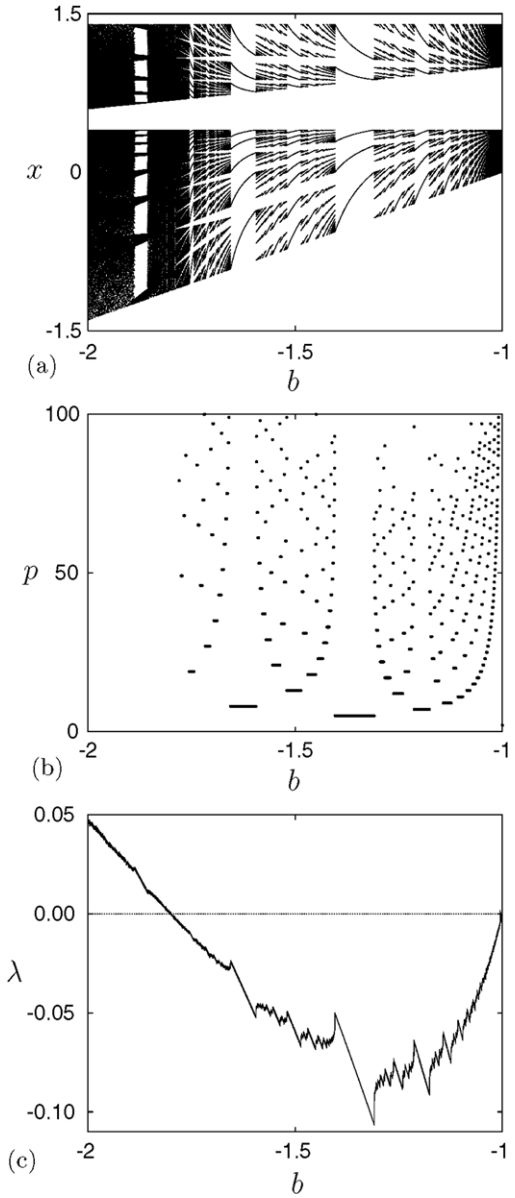

Figure 6. Bifurcation diagram, period diagram and Lyapunov exponent in the case $a = 0.2$, $\mu = 0.4$ under variation of one control parameter b.

attractors. It may be unexpected, but we will show that for all three scenarios presented in figures 6, 7 and 8 there exists a simple and unified explanation, which is based on two- and three-parametric bifurcations.

6.2. Emergence of stable periodic orbits

In order to explain the complex behaviour observed numerically, let us consider again the orbits $O_{\mathcal{LR}^n}$. As shown above, the existence areas of these orbits are bounded by the bifurcation

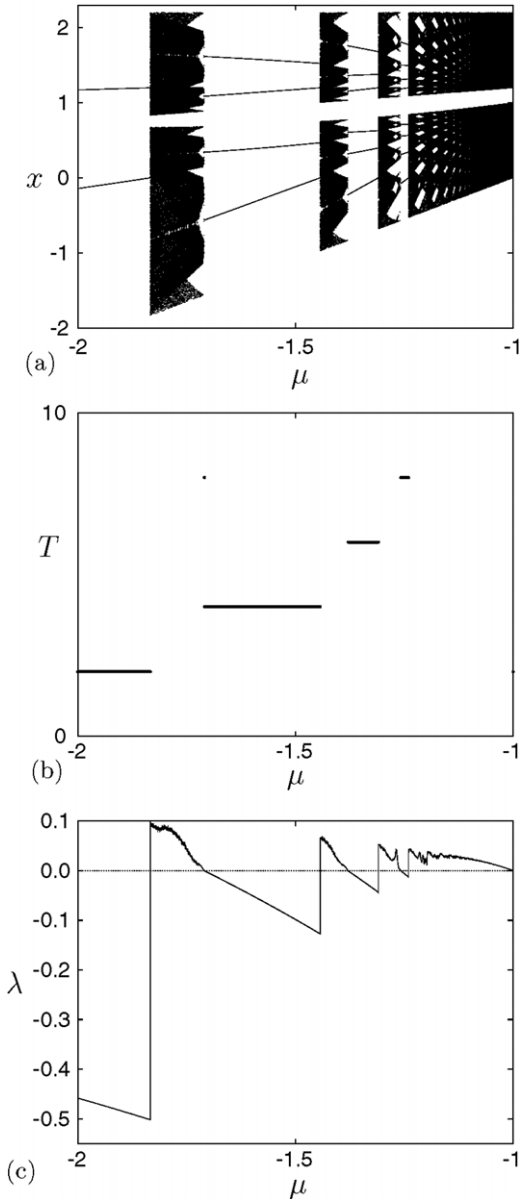

Figure 7. Bifurcation diagram, period diagram and Lyapunov exponent in the case $a = 0.2$, $\mu = 1.2$ under the variation of one control parameter b.

surfaces $\xi^{x_0,l}_{\mathcal{L}\mathcal{R}^n}$ and $\xi^{x_{n-1},r}_{\mathcal{L}\mathcal{R}^n}$, given by equations (9) and (10). In contrast to the case $a = 0$, where the existence and stability areas of $O_{\mathcal{L}\mathcal{R}^n}$ are identical, in the case $a \neq 0$ a periodic orbit may become unstable. In general, if $N_{\mathcal{L}}(\sigma)$ and $N_{\mathcal{R}}(\sigma)$ are the numbers of symbols $\mathcal{L}$ and $\mathcal{R}$ in the admissible symbolic sequence σ, then the Lyapunov exponent of O_σ is given by

$$\lambda_\sigma = \frac{N_{\mathcal{L}}(\sigma)\ln|a| + N_{\mathcal{R}}(\sigma)\ln|b|}{N_{\mathcal{L}}(\sigma) + N_{\mathcal{R}}(\sigma)}. \tag{18}$$

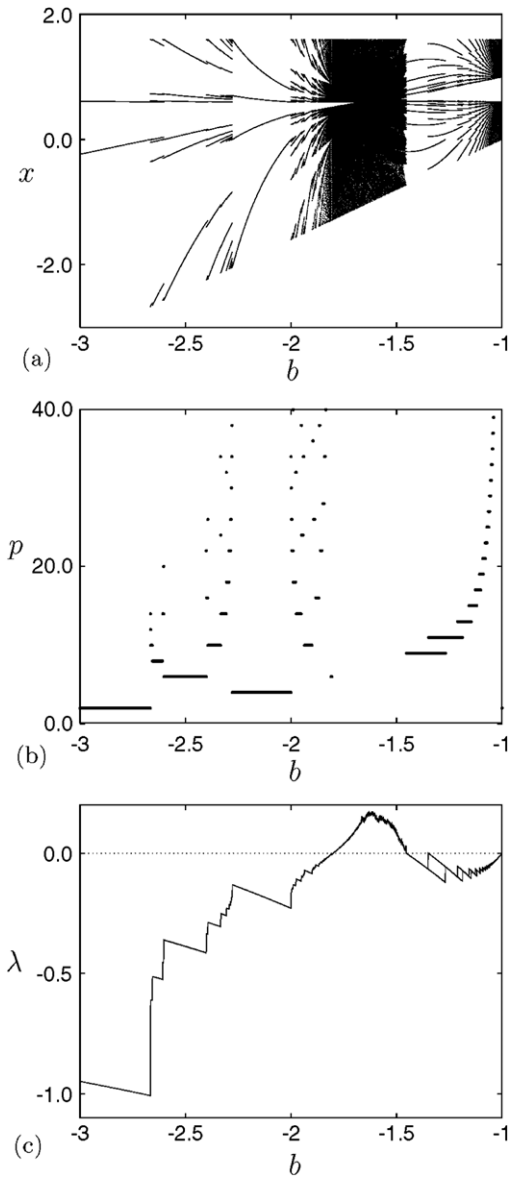

Figure 8. Bifurcation diagram, period diagram and Lyapunov exponent in the case $a = -0.05$, $\mu = 0.6$ under the variation of one control parameter b. Note the intervals with coexisting attractors in the right part of the figure.

Using the condition

$$\lambda_{\mathcal{LR}^n} = \frac{\ln|a| + n\ln|b|}{n+1} = 0 \tag{19}$$

we obtain that $O_{\mathcal{LR}^n}$ loses its stability along the line

$$b_{\mathcal{LR}^n} = -|a|^{-1/n}. \tag{20}$$

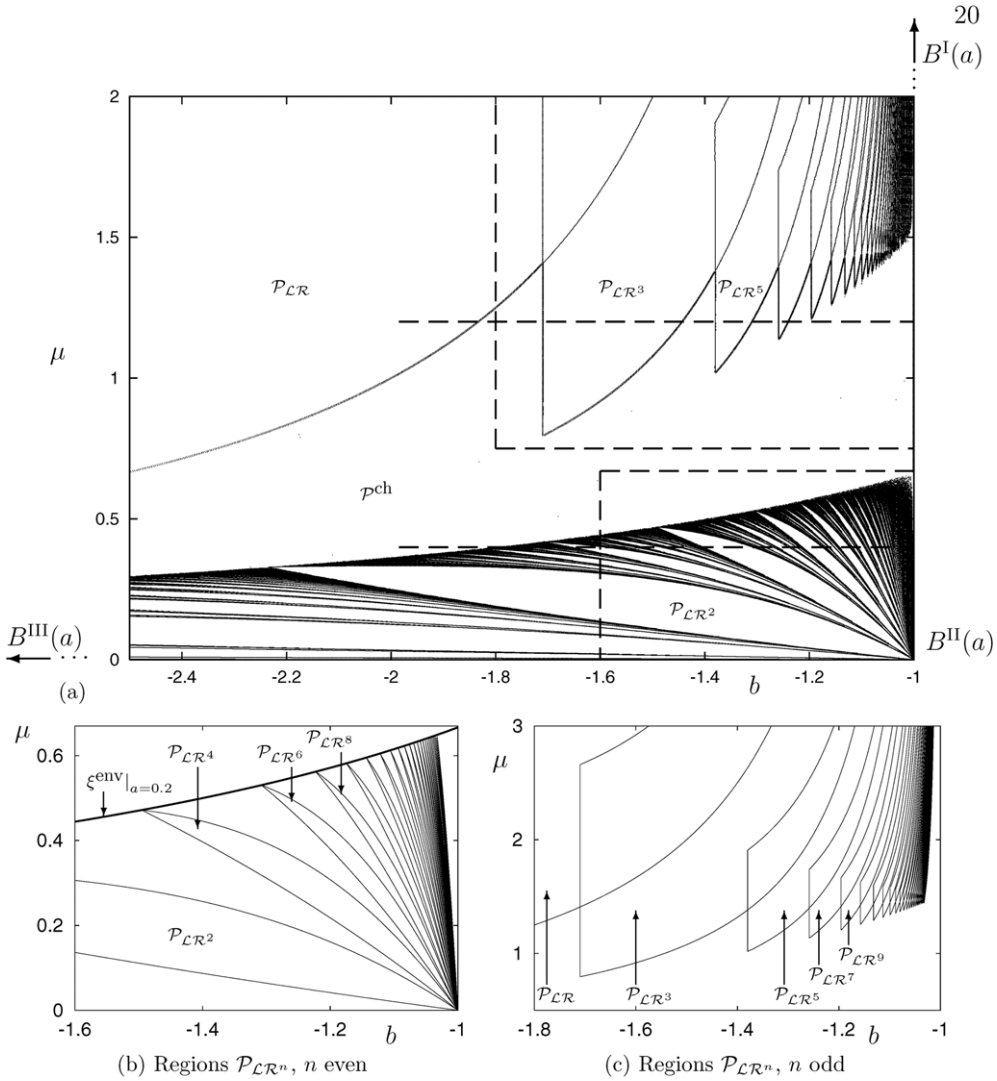

Figure 9. Bifurcation structure of the plane $b \times \mu$ in the case $a = 0.2$. (*a*) Results obtained numerically, (*b*), (*c*) analytical calculated areas $\mathcal{P}_{\mathcal{LR}^n}$ for $n \leqslant 52$. Horizontal dashed lines in (*a*) correspond to figures 6 and 7. Analytic results corresponding to the rectangles marked in (*a*) are shown in (*b*) and (*c*), enlarged.

6.3. Big bang bifurcations

In order to explain the structure of the parameter plane $b \times \mu$ for the case $a \neq 0$ we have now to consider the relative positions of the areas $\mathcal{P}_{\mathcal{LR}^n}$ with respect to each other. As in the case $a = 0$, we state that the points $B^{\mathrm{I}}(a)$ and $B^{\mathrm{II}}(a)$ represent big bang bifurcations and that each area $\mathcal{P}_{\mathcal{LR}^n}$ starts at one of these points. However the type of these big bang bifurcations is different for the cases $a > 0$ and $a < 0$, see figures 9 and 10. More precisely, the following can be proved analytically.

(i) In the case $a > 0$ the point $B^{\mathrm{I}}(a)$ represents a period increment big bang bifurcation with coexistence of attractors, and the point $B^{\mathrm{II}}(a)$ a period adding big bang bifurcation.

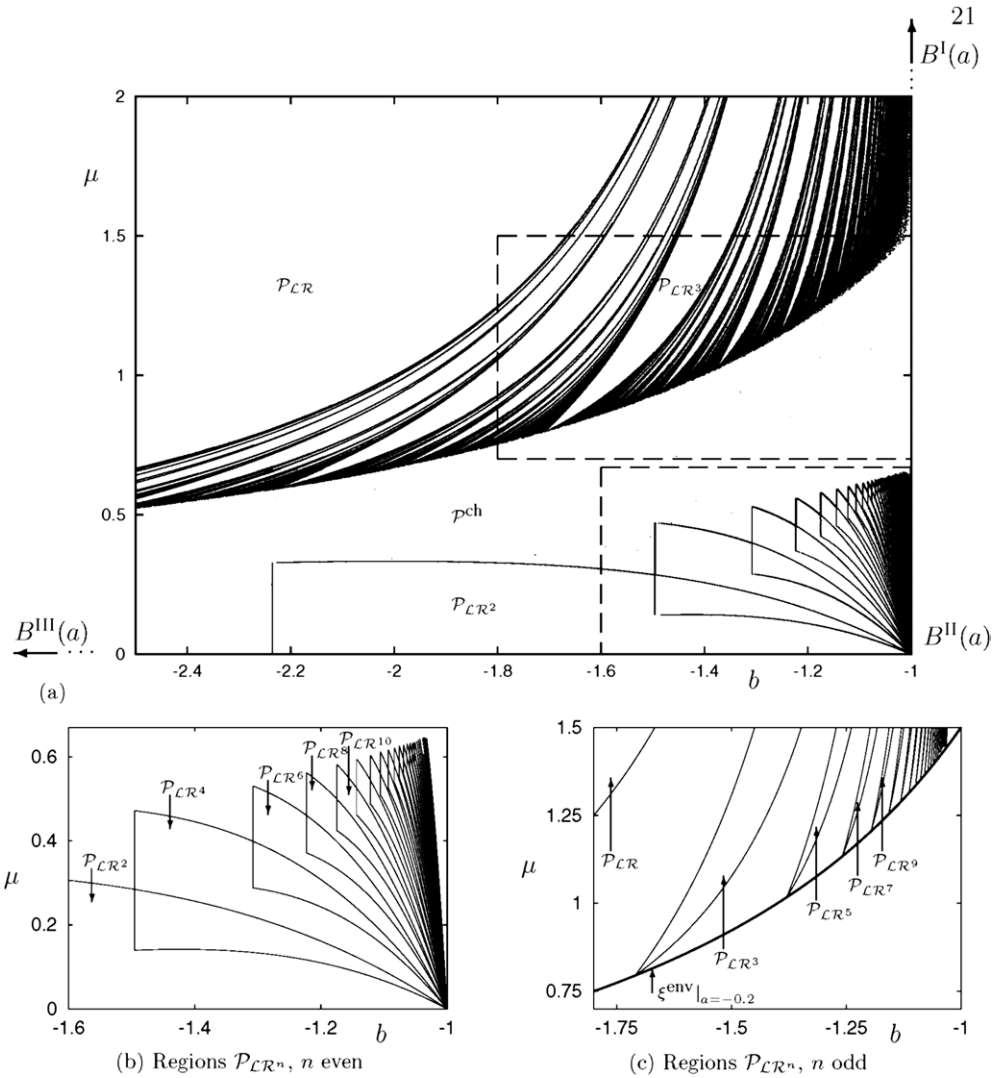

Figure 10. Bifurcation structure of the plane $b \times \mu$ in the case $a = -0.2$. (*a*) Results obtained numerically, (*b*), (*c*) analytical calculated areas $\mathcal{P}_{\mathcal{LR}^n}$ for $n \leqslant 52$.

(ii) In the case $a = 0$ both points represent period increment big bang bifurcations.
(iii) In the case $a < 0$ the point $B^{\mathrm{I}}(a)$ represents a period adding big bang bifurcation and the point $B^{\mathrm{II}}(a)$ a period increment big bang bifurcation with coexistence of attractors.

These facts represent the main result of this section and have to be discussed in futher detail. The case $a = 0$ has already been explained in the previous section. Let us now consider the point $B^{\mathrm{I}}(a)$ in the case $a > 0$. Similarly to the case $a = 0$, the areas $\mathcal{P}_{\mathcal{LR}^{2n+1}}$ originate from this point. However, in contrast to the case $a = 0$, it can be easily shown that for $a > 0$ each two subsequent areas $\mathcal{P}_{\mathcal{LR}^{2n+1}}$ and $\mathcal{P}_{\mathcal{LR}^{2n+3}}$ overlap (see figure 9(*c*)). Therefore each 1D parameter scan around this point (for a sufficient large value of μ) is similar to the one presented in figure 11(*a*). As shown in this figure, for each two subsequent even numbers there is a parameter interval where the attractors with corresponding periods coexist. Analogous

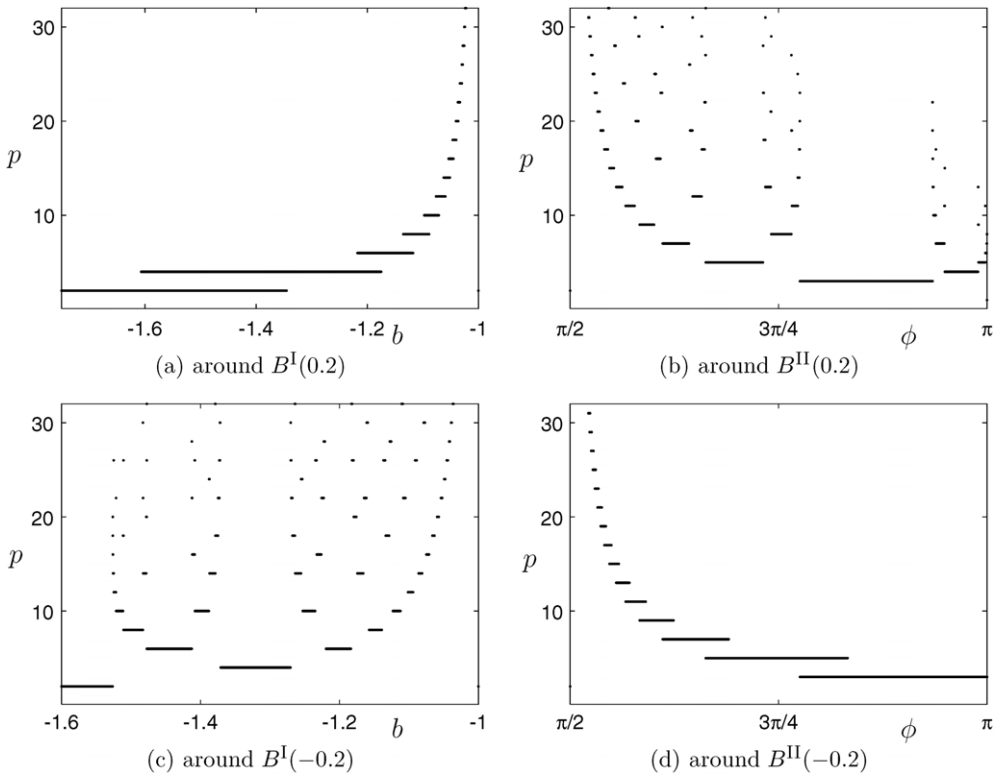

Figure 11. 1D bifurcation scenarios in the plane $b \times \mu$ around the border of the vicinity of big bang bifurcation points $B^{\mathrm{I}}(a)$ (left) and $B^{\mathrm{I}}(a)$ (right) for positive and negative values of a. In the case $a > 0$, $B^{\mathrm{I}}(a)$ represents a period increment big bang bifurcation with coexistence of attractors and $B^{\mathrm{I}}(a)$ a period adding one. In the case $a < 0$ the situation is the reverse.

behaviour can be observed around the point $B^{\mathrm{II}}(a)$ for $a < 0$ (i.e. for a sufficiently small value of μ, figure 11(*d*)).

The behaviour around the point $B^{\mathrm{II}}(a)$ for $a > 0$ is more complex. Equations (9) and (10) imply that in this case there is some 'free space' between each of the two subsequent areas $\mathcal{P}_{\mathcal{LR}^{2n}}$ and $\mathcal{P}_{\mathcal{LR}^{2n+2}}$. It can be shown that this is the space in which the areas $\mathcal{P}_\sigma$ lie, whereby the sequence σ can be generated from the sequences $\mathcal{LR}^{2n}$ and $\mathcal{LR}^{2n+2}$ using the infinite symbolic adding scheme, as described in section 3.2. These sequences play the most important role for the description of the bifurcation phenomena occurring in system (2)[3]. Note that there exist

[3] Note that there are several notations related to sequences similar to those we consider in this work. Firstly, in [34,35], the orbits corresponding to sequences $\mathcal{LR}^n$ are denoted as *maximal orbits*. Secondly, in [36] the orbits corresponding to sequences $\mathcal{L}^m\mathcal{R}^n$ are called *regular orbits*. Finally, in [20, 37] the orbits corresponding to the so-called *evenly distributed sequences* are considered. Hereby a sequence is denoted as evenly distributed if it consists only of syllables of only the forms $\mathcal{LR}^n$, $\mathcal{LR}^{n+1}$ or $\mathcal{L}^n\mathcal{R}$, $\mathcal{L}^{n+1}\mathcal{R}$. Obviously, sequences corresponding to maximal orbits are a special case of evenly distributed sequences, as well as the sequences corresponding to regular orbits in the case $m = 1$ or $n = 1$. It is important to emphasize two differences between evenly distributed sequences and sequences which we consider in this work. Firstly, due to the different mechanism leading to the emergence of periodic orbits in system (2) (see section 5.2), we consider sequences composed of syllables of the forms $\mathcal{LR}^n$, $\mathcal{LR}^{n+2}$ or $\mathcal{L}^n\mathcal{R}$, $\mathcal{L}^{n+2}\mathcal{R}$. Secondly, not each evenly distributed sequence can be generated by the infinite adding scheme. Consider for instance the sequences $\mathcal{LR}^n\mathcal{LR}^{n+2}\mathcal{LR}^n(\mathcal{LR}^{n+2})^2$ and $(\mathcal{LR}^n)^2(\mathcal{LR}^{n+2})^3$. Both of them contain the same syllables, but the first one can be generated by the infinite adding scheme, whereas the second one cannot.

some areas in the parameter space where system (2) has stable orbits corresponding to some other sequences (see for example the sequence $\mathcal{L}^2\mathcal{R}^3$ in figure 15), but in this work we will not investigate these orbits.

Due to the bijective mapping between the 2D parameter space and the space of symbolic sequences, it can be shown that between the areas $\mathcal{P}_{\mathcal{L}\mathcal{R}^{2n}}$ and $\mathcal{P}_{\mathcal{L}\mathcal{R}^{2n+2}}$ lies the area $\mathcal{P}_{\mathcal{L}\mathcal{R}^{2n}\mathcal{L}\mathcal{R}^{2n+2}}$, between $\mathcal{P}_{\mathcal{L}\mathcal{R}^{2n}}$ and $\mathcal{P}_{\mathcal{L}\mathcal{R}^{2n}\mathcal{L}\mathcal{R}^{2n+2}}$ lies the area $\mathcal{P}_{(\mathcal{L}\mathcal{R}^{2n})2\mathcal{L}\mathcal{R}^{2n+2}}$, etc. Hence, performing a 1D parameter scan around the point $B^{\mathrm{II}}(a)$ for $a > 0$, we observe a period adding scenario like the one presented in figure 11(*b*). Note that the behaviour occurring around the point $B^{\mathrm{I}}(a)$ for $a < 0$ is exactly the same (figure 11(*c*)).

In order to complete the description of the period adding big bang bifurcations occurring at the points $B^{\mathrm{I}}(a)$ for $a < 0$ and $B^{\mathrm{II}}(a)$ for $a > 0$, it is worth mentioning that in these cases not only the areas $\mathcal{P}_{\mathcal{L}\mathcal{R}^n}$, but also $\mathcal{P}_{\mathcal{L}^n\mathcal{R}}$ originate from the big bang bifurcation points. More precisely, in the case $a < 0$ from the point $B^{\mathrm{I}}(a)$ originate the areas $\mathcal{P}_{\mathcal{L}^{2n+1}\mathcal{R}}$, as well as the areas $\mathcal{P}_\sigma$, whereby the sequence σ can be generated from $\mathcal{L}^{2n+1}\mathcal{R}$ and $\mathcal{L}^{2n+3}\mathcal{R}$ using the infinite symbolic adding scheme. Similarly, in the case $a > 0$ from the point $B^{\mathrm{II}}(a)$ originate the areas $\mathcal{P}_{\mathcal{L}^{2n}\mathcal{R}}$ and the areas $\mathcal{P}_\sigma$, whereby the sequence σ can be generated from $\mathcal{L}^{2n}\mathcal{R}$ and $\mathcal{L}^{2n+2}\mathcal{R}$. Note that these areas emerge only in the case when the corresponding big bang bifurcation is of the period adding type. In the cases where the bifurcation is of the period increment type (with or without coexisting attractors), the corresponding sequences are not admissible in the influence area of this bifurcation.

6.4. Influence areas

As one can see from figures 9 and 10, in both cases $a > 0$ and $a < 0$, a large part of the investigated area $\mathcal{P}$ is covered by the influence areas $\Omega(B^{\mathrm{I}}(a))$ and $\Omega(B^{\mathrm{II}}(a))$. In contrast to the case $a = 0$, where the areas $\Omega(B^{\mathrm{I}}(0))$ and $\Omega(B^{\mathrm{II}}(0))$ are separated from each other by the smooth curve ξ_∞, in both cases $a > 0$ and $a < 0$ the areas $\Omega(B^{\mathrm{I}}(a))$ and $\Omega(B^{\mathrm{II}}(a))$ are separated from each other by an extended area $\mathcal{P}^{\mathrm{ch}}$ leading to a chaotic dynamics. The interior structure of this area is complex as well; there are one-band and multi-band attractors within. However, in this work we restrict ourselves to an investigation of periodic orbits caused by multi-parametric bifurcations. Therefore, the investigation of the structure of $\mathcal{P}^{\mathrm{ch}}$ is left for future work.

It turns out that the boundaries of the above-mentioned influence areas have different properties depending on the type of the corresponding big bang bifurcation. In the case of period increment big bang bifurcations with coexistence of attractors ($\Omega(B^{\mathrm{I}}(a))$ for $a > 0$ as well as $\Omega(B^{\mathrm{II}}(a))$ for $a < 0$), the influence areas cannot be calculated in a closed form, but only as

$$\Omega(B^{\mathrm{I}}(a))|_{a>0} = \bigcup_{n=0}^{\infty} \mathcal{P}_{\mathcal{L}\mathcal{R}^{2n+1}}, \tag{21}$$

$$\Omega(B^{\mathrm{II}}(a))|_{a<0} = \bigcup_{n=1}^{\infty} \mathcal{P}_{\mathcal{L}\mathcal{R}^{2n}}, \tag{22}$$

whereby the boundaries of the areas $\mathcal{P}_{\mathcal{L}\mathcal{R}^{2n+1}}$ and $\mathcal{P}_{\mathcal{L}\mathcal{R}^{2n}}$ are given by equations (9), (10) and (20). In contrast to the case $a = 0$, the boundaries of $\Omega(B^{\mathrm{I}}(a))$ for $a > 0$ as well as $\Omega(B^{\mathrm{II}}(a))$ for $a < 0$ represent a non-smooth curve. Remarkably, these boundaries consist of two types of bifurcation curves: along the curves of the first type the corresponding stable periodic orbit disappears, whereas along the curves of the second type it becomes unstable.

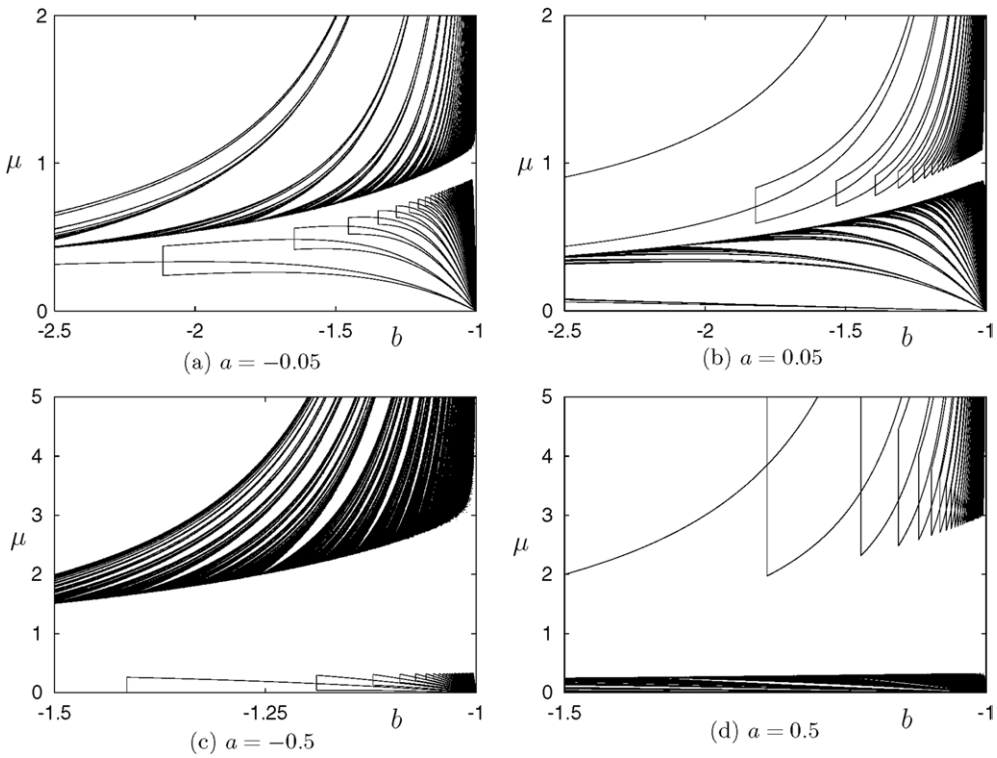

Figure 12. Influence areas of the big bang bifurcation points $B^{\mathrm{I}}(a)$ and $B^{\mathrm{II}}(a)$ in the plane $b \times \mu$ for several values of a. The influence areas shrink for increasing values of $|a|$, whereas the area $\mathcal{P}^{\mathrm{ch}}$ (lying in-between) grows. Note that the structure of figures (*a*) and (*c*) corresponds to the structure of figure 10, whereas the the structure of figures (*b*) and (*d*) corresponds to that of figure 9.

In the case of period adding big bang bifurcations the influence areas can be calculated in closed form:

$$\Omega(B^{\mathrm{I}}(a))\big|_{a<0} = \left\{(b,\mu) \;\middle|\; \mu > \frac{1-a}{a-b}\right\}, \tag{23}$$

$$\Omega(B^{\mathrm{II}}(a))\big|_{a>0} = \left\{(b,\mu) \;\middle|\; \mu < \frac{1-a}{a-b}\right\}. \tag{24}$$

Hereby the boundary surface ξ^{env} is defined by

$$\xi^{\mathrm{env}} = \left\{(a,b,\mu) \;\middle|\; -1 < a < 1, b < -1, \mu = \frac{1-a}{a-b}\right\} \tag{25}$$

and follows from the condition $f_l(f_r(0)) = f_r(f_l(0))$. Note that the curve ξ_∞ (see equation (11)) represents the intersection $\xi^{\mathrm{env}}|_{a=0}$ of the surface ξ^{env} with the plane $a = 0$. Investigating the behaviour of system (2) for increasing values of $|a|$, we observe that the influence areas $\Omega(B^{\mathrm{I}}(a))$ and $\Omega(B^{\mathrm{II}}(a))$ become smaller. In the case $a = 0$ these areas adjoin each other, so that there is no area $\mathcal{P}^{\mathrm{ch}}$ in between. For $|a| = 0.05$ (see figures 12(*a*) and (*b*)) the areas $\Omega(B^{\mathrm{I}}(a))$ and $\Omega(B^{\mathrm{II}}(a))$ cover the most part of $\mathcal{P}$, and the area $\mathcal{P}^{\mathrm{ch}}$ in between is comparatively small. As one can see from these figures, for any value of μ there are values of b where system (2) shows a periodic dynamics with arbitrary high periods. In contrast to this, for $|a| = 0.2$ (figures 9 and 10), the influence areas become smaller and for instance for

$\mu = 0.6$ system (2) is able to demonstrate either two-periodic or chaotic solutions. For further increasing values of $|a|$, the influence areas continue to shrink (as shown in figures 12(*c*) and (*d*) for the case $|a| = 0.5$). However, the areas do not vanish in the complete interval $|a| < 1$, and hence for any value $|a| < 1$ we are able to determine the values of the parameters b and μ leading to an arbitrary high period.

6.5. Numerical observations revisited

Now the behaviour presented in figures 6, 7 and 8 can be explained easily. The scenario shown in figure 6 is observed by performing a section of the 2D parameter space from the area $\mathcal{P}^{\mathrm{ch}}$ into the area $\Omega(B^{\mathrm{II}}(0.2))$, as shown in figure 9. In contrast to this, figure 7 corresponds to the area $\mathcal{P}^{\mathrm{ch}}$ with some periodic windows originating at $B^{\mathrm{I}}(0.2)$. In the presented case only four of these areas are crossed, therefore the period increment scenario is truncated after the period 8. Note that increasing the value of μ one would cross more of these areas and hence the period increment scenario would be truncated later. For larger values of μ the coexistence of attractors would be observed as well. Finally, the mixed scenario consisting of period adding and period increment with coexistence of attractors, presented in figure 8, emerges, because for $a = -0.05$ the presented interval $b \in [-3, -1]$, $\mu = 0.6$ crosses both influence areas $\Omega(B^{\mathrm{II}})(-0.05)$ and $\Omega(B^{\mathrm{II}})(-0.05)$ (see figure 12(*a*)).

Let us consider additionally the Lyapunov exponents in the case of the period adding scenarios presented in the right part of figure 7(*c*) and the left part of figure 8(*c*). If we interpret the Lyapunov exponents shown in these figures as a function $\lambda(b)$ of the parameter b, then this function is similar to the well-known Cantor–Lebesgue function. As shown above, the period increment scenario is caused by the subsequent cross-section of an infinite number of areas $\mathcal{P}_\sigma$, which start at the period adding big band bifurcations. For a fixed a equation (18) implies that within each of these areas the function $\lambda_\sigma(b)$ is given by $c_1 + c_2 \ln|b|$ with constant $c_{1,2}$. Hence, $\lambda_\sigma(b)$ is differentiable in each area $\mathcal{P}_\sigma$ and therefore almost everywhere (like the Cantor–Lebesgue function). However, $\lambda_\sigma(b)$ has almost everywhere a negative slope, in contrast to the Cantor–Lebesgue function, which is almost everywhere constant.

7. Three-parametric bifurcations

Until now we considered the structure of the 2D parameter space and demonstrated that the structure is dominated by a few co-dimension-2 bifurcations. However, the complete parameter space of the investigated system is three-dimensional, therefore the results obtained so far have to be considered in this more general context.

7.1. Three-parametric bifurcation $B^{\mathrm{II}}(0)$

Let us consider for instance the bifurcations occurring along the line $B^{\mathrm{II}}(a)$ in the 3D parameter space. As shown above, for $a < 0$ each point on this line represents a period adding big bang bifurcation, whereas for $a > 0$ it represents a period increment big bang with coexistence of attractors. For this reason, the bifurcation occurring at the point $B^{\mathrm{II}}(0)$ (i.e. in the 'switching' case $a = 0$) is a three-parametric bifurcation.

The description of the structure of the 3D parameter space in the vicinity of the three-parametric bifurcation point $B^{\mathrm{II}}(0)$ is the next task that we have to deal with. This task turns out to be really complex, although the case $a = 0$ is already described in section 5. However, in this section we described the point $B^{\mathrm{II}}(0)$ from a pure two-dimensional point of view, and therefore were not able to recognize the real complexity of the phenomenon. This complexity

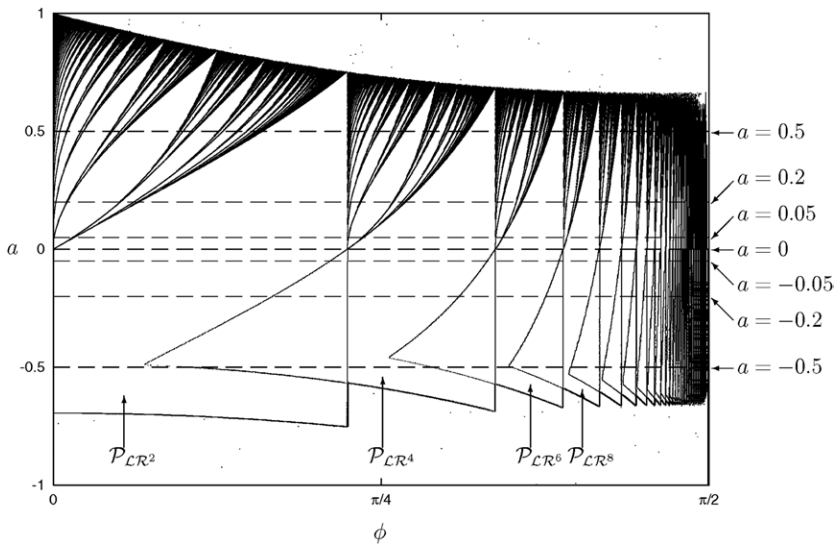

Figure 13. Bifurcation structure of the cylindric surface around the point $B^{\mathrm{II}}(0)$. The marked horizontal lines correspond to the planes $b \times \mu$ shown in figures 4, 9, 10 and 12.

is reflected in figure 13. In this figure the bifurcation structure in the cylindric surface $a \times \phi$ around the line $B^{\mathrm{II}}(a)$ in the 3D parameter space $a \times b \times \mu$ is shown, where we use the polar representation of the parameters b and μ, i.e. $b = -1 - R\cos(\phi)$, $\mu = R\sin(\phi)$. Recall, that the values $a = -0.5$, $a = -0.2$, $a = -0.05$, $a = 0$, $a = 0.05$, $a = 0.2$ and $a = 0.5$ shown in this picture as horizontal lines correspond to figures 4, 9, 10 and 12.

As one can see from figure 13, the points located along the line $a = 0$ form an infinite sequence of period adding big bang bifurcations. These points represent the intersections of the bifurcation curves $\xi^{x_0,l}_{\mathcal{LR}^n}|_{a=0}$ in the plane $a = 0$ with the cylindric surface mentioned above. This fact can be explained taking the following into consideration. Firstly, from equations (9) and (10) it follows that for all n the bifurcation surfaces $\xi^{x_0,l}_{\mathcal{LR}^n}$ and $\xi^{x_{n+1},r}_{\mathcal{LR}^{n+2}}$ intersect along the curve $\xi^{x_0,l}_{\mathcal{LR}^n}|_{a=0}$. Secondly, for any admissible symbolic sequence σ, which can be derived from $\mathcal{LR}^n$ and $\mathcal{LR}^{n+2}$ using the infinite adding scheme, the bifurcation surfaces bounding the area $\mathcal{P}_\sigma$ intersect along the curve $\xi^{x_0,l}_{\mathcal{LR}^n}|_{a=0}$ as well.

Additionally, the described structure of the 3D parameter space is shown in figure 14. This 3D representation combines the results shown in previous figures. Namely, the three horizontal planes $a = -0.2$, $a = 0$ and $a = 0.2$ are shown in figures 10, 4 and 9, whereas the surface of the cylinder is shown in figure 13. As one can see from figure 14, all the bifurcation surfaces forming this structure originate from the line $B^{\mathrm{II}}(a)$, whereby the point $B^{\mathrm{II}}(0)$ belongs to all these surfaces and represents a three-parametric or co-dimension-3 bifurcation.

Three-parametric bifurcations of this type are already reported in [30, 31]. As described in the cited works, a three-parametric bifurcation of this type has two characteristic manifolds in the 3D parameter space, a one-dimensional and a two-dimensional one. Each point on the 1D characteristic manifold except the three-parametric bifurcation point itself represents a point of a two-parametric bifurcation, which is a period adding big bang on one side of the 2D characteristic manifold and a period increment big bang with coexisting attractors on the other side. Additionally, in the 2D characteristic manifold the three-parametric bifurcation represents a pure period increment big bang bifurcation. Hereby, each of the infinite number

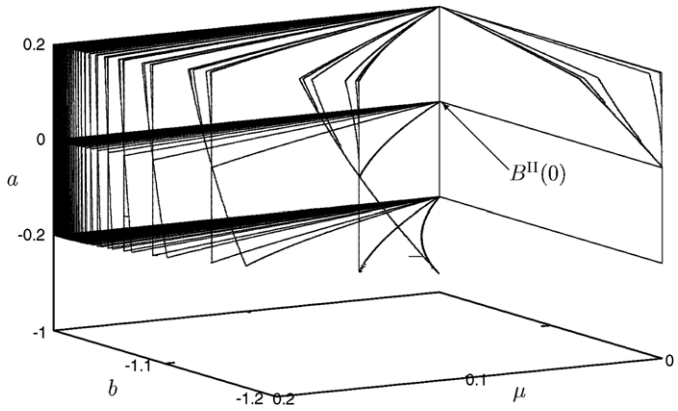

Figure 14. Structure of parameter space in the 3D vicinity of the three-parametric bifurcation point $B^{II}(0)$.

of bifurcation curves generated by this pure period increment big bang bifurcation represents a domain of period adding big bang bifurcations.

As one can see, the three-parametric bifurcation at the point $B^{II}(0)$ fits the presented general description exactly. The 1D characteristic manifold of this bifurcation is given by the line $B^{II}(a)$ and the 2D characteristic manifold by the plane $a = 0$. Above the 2D manifold, the big bang bifurcations are of the period adding type (compare figure 9); in this manifold they are of the period increment type (figure 4), and below the manifold they are of the period increment type with coexisting attractors (figure 10). Additionally, the bifurcation curves $\xi_{\mathcal{LR}^n}^{x_0,l}|_{a=0}$ in the 2D characteristic manifold represent curves in the 3D parameter space, where period adding big bang bifurcations occur (see figure 13).

7.2. $B^{I}(0)$ and $B^{II}(0)$

Like the point $B^{II}(0)$, also the point $B^{I}(0)$ represents a three-parametric bifurcation as well. Moreover, it turns out that the type of this bifurcation is the same as the bifurcation at $B^{II}(0)$, and that the 2D characteristic manifolds of both bifurcations lie in the same plane $a = 0$. The only difference between these two bifurcations is the 'direction' of their 1D characteristic manifolds. For the bifurcation at $B^{I}(0)$ the points at the 1D characteristic manifolds represent the period adding big bang bifurcation for $a < 0$ (unlike the case for $B^{II}(0)$ where it is for $a > 0$). Analogously, the points at the 1D characteristic manifolds represent period increment big bang bifurcation with coexisting attractors for $a > 0$ instead of $a < 0$, as is the case for $B^{II}(0)$. Concerning all other aspects both bifurcation points $B^{I}(0)$ and $B^{II}(0)$ are identical.

In conclusion, let us emphasize the importance of the obtained results. As one can see, the 2D bifurcation structures shown in figures 4, 9 and 10 are quite complex. The 1D bifurcation diagrams like the ones presented in figures 6, 7 and 8 are complex as well. However, all these results can be explained taking into consideration only two three-parametric bifurcations occurring at $B^{I}(0)$ and $B^{II}(0)$.

7.3. Remarks on $B^{III}(0)$

As for the case $a = 0$, for any $a \neq 0$ the point $B^{III}(a)$ represents a big bang bifurcation as well. However, the type of this big bang is totally different from all big bang bifurcations investigated

so far. It can be shown that the existence areas of all periodic orbits emerging at the point of the period increment big bang bifurcation with coexisting attractors (i.e. at $B^{\mathrm{II}}(0)$ for $a > 0$ and $B^{\mathrm{I}}(0)$ for $a < 0$) converge towards this point. As stated in section 6.2 (see equation (20)), for any n there exists a sufficiently large negative value b, so that the corresponding periodic orbit becomes unstable. Therefore, all periodic orbits originating from the corresponding period increment big bang bifurcation with coexisting attractors are unstable in the vicinity of $B^{\mathrm{III}}(a)$. Hence, this type of big bang bifurcation, causing the occurence of coexisting unstable periodic orbits, has important consequences, especially because it seems to be closely related to the emergence of chaotic attractors. It can also be shown that the properties of this bifurcation in system (2) change at $a = 0$. Therefore, the point $B^{\mathrm{III}}(0)$ represents a three-parametric bifurcation. However, a detailed investigation of the bifurcation occurring at $B^{\mathrm{III}}(0)$ remains for future work.

8. Plane $a \times b$

8.1. General remarks

Now let us consider the results obtained so far from a more practical perspective. As shown above, the structure of the 3D parameter of system (2) is strongly dominated by a few three-parametric bifurcations. However, as one can see for instance from figures 2, 6, 7, 8 and 11, it is almost impossible to recognize this structure if one investigates the behaviour of this system under variation of only one parameter. Investigating 2D parameter planes instead, one has a much better view of several dynamical features. However, if the investigated 2D parameter subspaces cross the characteristic manifolds of the three-parametric bifurcations, the observed structures become strange and may also be very difficult to interpret. Note that the structures presented in figures 4, 9, 10, and 12 can be interpreted easily mainly because the presented parameter planes are parallel to the 2D characteristic manifolds of $B^{\mathrm{I}}(0)$ and $B^{\mathrm{II}}(0)$. In practical applications, the 2D characteristic manifolds are not necessarily planes, and their location in the parameter space is not *a priori* known. For this reason, it is important to demonstrate what the bifurcation structures may look like if one investigates the 2D parameter spaces not parallel to the 2D characteristic manifolds of three-parametric bifurcations.

Note further that the discussion presented in the following has two objectives. On the one hand, it has to aid the investigation of other dynamical systems whose behaviour is influenced by three-parametric bifurcations of the type presented in this work. If in some dynamical system the observed bifurcation structures are similar to those discussed in the following, one can assume that in this system three-parametric bifurcations occur and one has to determine their characteristic manifolds in order to understand these bifurcation structures. On the other hand, the following examples demonstrate how the observed structures have to be interpreted taking into account the knowledge about the three-parametric bifurcations presented above.

8.2. Example 1: case $\mu = 1/2$

As a typical example of the structure of the plane $a \times b$ let us consider the situation in the case $\mu = 1/2$. As one can see from figure 15, this structure is far from being trivial. It is clearly observable that there are two main structure-forming elements in this figure.

The first one is the straight line

$$a^{\mathrm{env}}(b, \mu) = \frac{\mu b + 1}{\mu + 1} = \xi^{\mathrm{env}}\big|_{\mu=1/2} \tag{26}$$

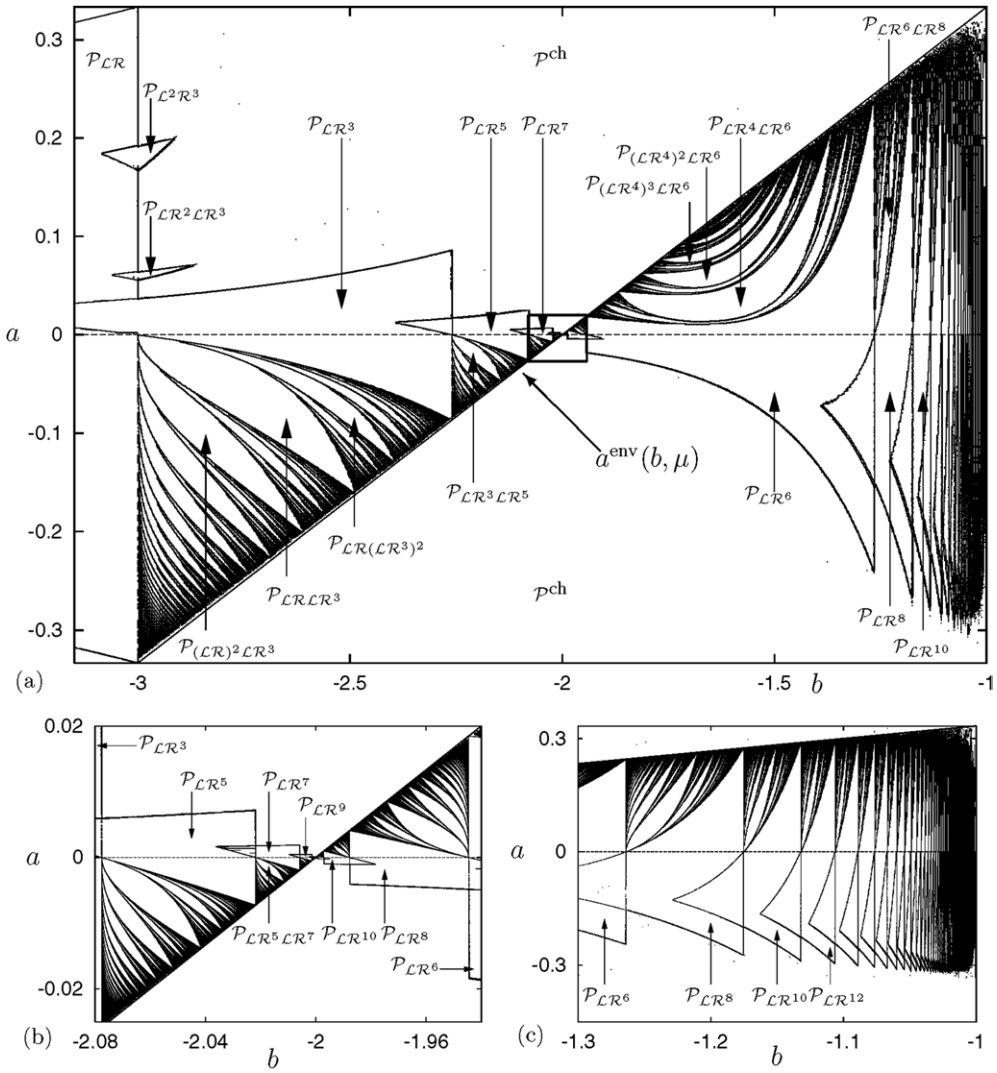

Figure 15. Complex bifurcation structures (*a*) in the plane $a \times b$ for the case $\mu = 0.5$ get a simple explanation based on the influence areas of the three-parametric bifurcations occurring at $B^{\mathrm{I}}(0)$ and $B^{\mathrm{II}}(0)$ in the 3D parameter space $a \times b \times \mu$. The rectangle marked in (*a*) is shown enlarged in (*b*), the right part of (*a*)—in (*c*).

and the second one is the horizontal line $a = 0$. The meaning of these two elements can be explained taking into account the results of the previous sections. Firstly, the line $a^{\mathrm{env}}(b, \mu)$ represents the border between the influence areas $\Omega(B^{\mathrm{I}}(0))|_{\mu=1/2}$ and $\Omega(B^{\mathrm{II}}(0))|_{\mu=1/2}$ of both the three-parametric bifurcations described above. Secondly, the line $a = 0$ represents the intersection of the presented plane $a \times b$ with the 2D characteristic manifolds of the three-parametric bifurcations occurring at $B^{\mathrm{I}}(0)$ and $B^{\mathrm{II}}(0)$.

In order to understand the bifurcation structure of the plane $a \times b$ presented in figure 15, note that the horizontal line $a = 0$ in this figure is identical with the line $\mu = 1/2$ marked in figure 4. As shown in figure 4, the accumulation curve ξ^{∞} intersects the line $\mu = 1/2$ at $b = -2$. As one can see, this point represents the accumulation point in figures 15(*a*) and (*b*).

Recall that the areas $\mathcal{P}_{\mathcal{LR}^{2n+1}}$ for all n are located above the accumulation curve ξ^{∞} shown in figure 4. Therefore, these areas belong to the structure presented in figure 15 as well. Here, above the line $a^{\mathrm{env}}(b,\mu)$ these areas have some triangle-like shapes and overlap pairwise for each two subsequent numbers n and $n+1$. The overlapping areas lie above the line $a=0$, because they belong to the influence area $\Omega(B^{\mathrm{I}}(0))$, and according to the direction of the 1D characteristic manifold of this three-parametric bifurcation, the coexistence of attractors takes place for $a>0$. Note additionally that in figure 15(*a*) only the first few areas in the sequence $\mathcal{P}_{\mathcal{LR}^{2n+1}}$ can be seen (marked are the areas $\mathcal{P}_{\mathcal{LR}}$, $\mathcal{P}_{\mathcal{LR}^3}$, $\mathcal{P}_{\mathcal{LR}^5}$ and $\mathcal{P}_{\mathcal{LR}^7}$). However, in the vicinity of the accumulation point $a=0$, $b=-2$ there exist areas $\mathcal{P}_{\mathcal{LR}^{2n+1}}$ with arbitrary n (see the enlargement shown in figure 15(*b*)).

Along the line $a=0$ we observe in figures 15(*a*) and (*b*) a sequence of period adding big bang bifurcations. As stated above, these bifurcations occur at points where the bifurcation curves forming the period increment scenario in the 2D characteristic manifold intersect the presented plane $a\times b$. Therefore, the corresponding points b_n can be found solving for the considered value $\mu=1/2$ the equation

$$\mu=-\frac{(b_n)^n\quad-1}{(b_n)^{n+1}-1}, \tag{27}$$

which follows directly from equation (9). For even numbers n the solutions of this equation lie in the interval $[-3,-2]$ and form for increasing n a sequence which converges to $b=-2$. Because the corresponding period adding big bang bifurcations belong to the influence area $\Omega(B^{\mathrm{I}}(0))$, the period adding structures induced by these bifurcations lie below the line $a=0$. According to the results discussed above, these structures consist of the areas $\mathcal{P}_{\sigma}$, whereby the sequences σ can be derived from $\mathcal{LR}^{2n+1}$ and $\mathcal{LR}^{2n+3}$ using the infinite adding scheme (for this reason in [38] the sequences $\mathcal{LR}^{2n+1}$ and $\mathcal{LR}^{2n+3}$ are denoted as the generating sequences of the corresponding period adding big bang bifurcation). For instance, at the point $a=0$, $b=b_1=-3$ we observe the period adding big bang bifurcation with the generating sequences $\mathcal{LR}$ and $\mathcal{LR}^3$. As shown in figure 15(*a*), between $\mathcal{P}_{\mathcal{LR}}$ and $\mathcal{P}_{\mathcal{LR}^3}$ we observe the area $\mathcal{P}_{\mathcal{LRLR}^3}$, between $\mathcal{P}_{\mathcal{LR}}$ and $\mathcal{P}_{\mathcal{LRLR}^3}$ the area $\mathcal{P}_{(\mathcal{LR})^2\mathcal{LR}^3}$, etc. Similarly, between $\mathcal{P}_{\mathcal{LR}^3}$ and $\mathcal{P}_{\mathcal{LR}^5}$ the area $\mathcal{P}_{\mathcal{LR}^3\mathcal{LR}^5}$ can be observed, which begins at the period adding big bang bifurcation point $a=0$, $b=b_3\approx-2.259\,921$.

A similar situation takes place below the line $a^{\mathrm{env}}(b,\mu)$, i.e. in the influence area $\Omega(B^{\mathrm{II}}(0))|_{\mu=1/2}$. For $a<0$ we observe the overlapping areas $\mathcal{P}_{\mathcal{LR}^n}$ with even numbers n (in figure 15(*a*) the areas $\mathcal{P}_{\mathcal{LR}^6}$, $\mathcal{P}_{\mathcal{LR}^8}$ and $\mathcal{P}_{\mathcal{LR}^{10}}$ are marked). At the corresponding points along the line $a=0$ the period adding big bang bifurcations occur, which lead to the period adding structures between the lines $a=0$ and $a^{\mathrm{env}}(b,\mu)$. For instance, the area $\mathcal{P}_{\mathcal{LR}^6\mathcal{LR}^8}$ begins at the big bang bifurcation occurring at the point $a=0$, $b=b_6\approx-1.263\,8376$. Solving equation (27) for $b\in[-1.5,-1]$ and increasing even numbers n, we can calculate the parameter values for all further period adding big bang bifurcations which occur in this interval and accumulate towards $b=-1$. This explains the bifurcation structure in the right part of figure 15(*a*), which is also shown enlarged in figure 15(*c*). Additionally, solving equation (27) for $b\in[-2,-1.5]$ and increasing even numbers n, we can also calculate the parameter values for further period adding big bang bifurcations which occur in this interval and accumulate towards $b=-2$. This explains the bifurcation structure in the middle of figure 15(*a*) and consequently in the right part of the enlargement shown in figure 15(*b*).

As one can see, most features of the bifurcation structure in the presented region of the plane $a\times b$ are explained so far. However, there is one difference between the areas below and above the line $a^{\mathrm{env}}(b,\mu)$ (i.e. between the influence areas $\Omega(B^{\mathrm{I}}(0))|_{\mu=1/2}$ and $\Omega(B^{\mathrm{II}}(0))|_{\mu=1/2}$), which is still not explained. Namely, above the line $a^{\mathrm{env}}(b,\mu)$ we observe a

sequence of areas $\mathcal{P}_{\mathcal{LR}^{2n+1}}$, which begins in the left part of figure 15(*a*) with $n = 0$ and converges for $n \to \infty$ towards $b = -2$. In contrast to this, below the line $a^{\mathrm{env}}(b, \mu)$ we observe two sequences of areas $\mathcal{P}_{\mathcal{LR}^{2n}}$. Both of them begin with $n = 3$, i.e. with $\mathcal{P}_{\mathcal{LR}^6}$. For $n \to \infty$ the first of these sequences converges to the right towards $b = -1$ and the second one to the left towards $b = -2$. This difference between the structure of the influence areas $\Omega(B^{\mathrm{I}}(0))|_{\mu=1/2}$ and $\Omega(B^{\mathrm{II}})(0)|_{\mu=1/2}$ is remarkable and seems to contradict the fact that the properties of both three-parametric bifurcations occurring at $B^{\mathrm{I}}(0)$ and $B^{\mathrm{II}}(0)$ are exactly the same.

The difference mentioned above is related to the fact that, for the considered value $\mu = 1/2$, equation (27) has one real solution b_n for each odd number n, two real solutions $b_n^{1,2}$ for even numbers $n > 4$ and no real solutions for $n = 2$ as well as for $n = 4$. In order to explain this, let us consider again figure 4. As one can see from this figure, for all odd numbers n the curves $\xi^{x_0,l}_{\mathcal{LR}^n}|_{a=0}$ are monotone and therefore intersect the horizontal line $\mu = 1/2$ exactly at one point. These points form the sequence of big bang bifurcations in the interval $[-3, -2]$ and are related to the areas $\mathcal{P}_{\mathcal{LR}^{2n+1}}$ (located in $\Omega(B^{\mathrm{I}}(0))|_{\mu=1/2}$).

In contrast to this, the curves $\xi^{x_0,l}_{\mathcal{LR}^{2n}}|_{a=0}$ are not monotone but have a maximum. Therefore, for a specific value of μ each of these curves may possess two, one or no intersections with the horizontal line μ. In particular, the curves $\xi^{x_0,l}_{\mathcal{LR}^2}|_{a=0}$ and $\xi^{x_0,l}_{\mathcal{LR}^4}|_{a=0}$ lie completely below the considered value $\mu = 1/2$. For this reason, equation (27) has no solutions for $n = 2$ and $n = 4$. Note additionally, that for each n the curve $\xi^{x_0,l}_{\mathcal{LR}^{2n+2}}|_{a=0}$ lies above the curve $\xi^{x_0,l}_{\mathcal{LR}^{2n}}|_{a=0}$. Hence, the corresponding intersection points with the line $\mu = 1/2$ form two sequences, one of them converging towards $b = -2$ and the other one towards $b = -1$, as described above.

Note that not all bifurcation phenomena observable in system (2) can be explained based only on the three-parametric bifurcations occurring at $B^{\mathrm{I}}(0)$ and $B^{\mathrm{II}}(0)$. For instance, in figure 15(*a*) two areas $\mathcal{P}_{\mathcal{L}^2\mathcal{R}^3}$ and $\mathcal{P}_{\mathcal{LR}^2\mathcal{LR}^3}$ are shown, which do not belong to the influence areas of these bifurcations. However, most features presented in this figure, including the self-similarity of its structure, could be explained due to the influence of these two bifurcations. Note that the bifurcations do not occur in the considered parameter plane, but influence it strongly. In our opinion, it is not possible to explain the structure of this plane based only on the bifurcation phenomena occurring within this plane. This situation is similar to the investigation of the 1D bifurcation scenarios (i.e. scenarios under variation of one system parameter). This mode of operation is suitable for understanding the occurring phenomena, as long as they are not influenced by two-parametric bifurcations. In the latter case, it is much more preferable to investigate these two-parametric bifurcations and their influence areas, which are typically easier to understand. Only after this one has to reconsider the original 1D scenarios, which then turn out to represent 1D cross-sections of 2D influence areas. A similar situation is reported above. Due to the presence of three-parametric bifurcations, the 2D parameter sub-spaces like the plane presented in figure 15(*a*) have to be considered not by themselves, but as the cross-sections of the 3D influence areas.

As a last remark related to the example presented above, let us emphasize that the situation described above may be typical when dealing with systems showing multi-parametric bifurcations. System (2) possesses in the region $\mathcal{P}$ two three-parametric bifurcations of the same type, but the effects caused by these bifurcations in the parameter sub-space (plane $a \times b$ for $\mu = 1/2$) are different. However, if we observe two multi-parametric bifurcations of the same type, it means merely that the structure of their vicinities is the same. In particular, for two-parametric bifurcations, the number of the bifurcation curves starting at these points is the same, as well as the order of the several asymptotic dynamics, bounded by these curves. However, this equivalence holds only in a topological sense; it means that the structure emerging at the bifurcation point remains the same within the complete influence area, but the curvature

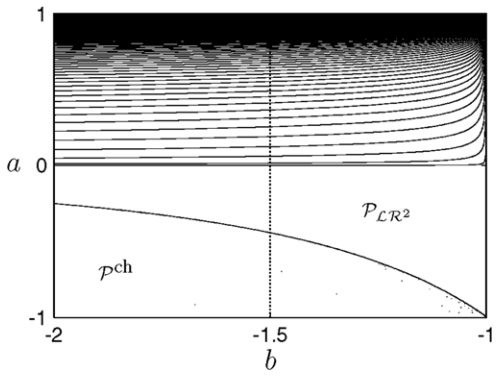

Figure 16. Bifurcation structure of the plane $a \times b$ in the case $\mu = 10^{-4}$. This structure can be easily misinterpreted as being caused by a period increment big bang bifurcation, but in fact is caused by a period adding big bang bifurcation.

and shape of the specific bifurcation curves may be different. An illustrative example of this behaviour is given by the bifurcation structure of the plane $a = 0$, where both 2D characteristic manifolds of the three-parametric bifurcations occurring at $B^{\mathrm{I}}(0)$ and $B^{\mathrm{II}}(0)$ are located. Note that the same property can be observed not only by the two-parametric but by any multi-parametric bifurcations as well.

8.3. Example 2: case $\mu = 10^{-4}$

In the previous example we have demonstrated how the complex bifurcation structures in 2D parameter subspaces can be explained taking into account the knowledge about three-parametric bifurcations and their influence on the structure of the complete 3D parameter space. In the next example we will demonstrate how such structures can be easily misunderstood and wrongly interpreted, if one does not take this knowledge into consideration.

Figure 16 shows the structure of the plane $a \times b$ in the vicinity of $B^{\mathrm{II}}(0)$ for a small value $\mu = 10^{-4}$. Investigating this structure based on the dependence on only one parameter, we observe bifurcation scenarios like the one presented in figure 17. For $a > 0$ this scenario looks similar to the usual period increment scenario, for instance, the one presented in figures 2(a) and (c). For $a < 0$ only two asymptotic dynamics are observed, namely, chaotic attractors and the periodic orbit $O_{\mathcal{LR}^2}$. For $a > 0$ we observe the areas $\mathcal{P}_{\mathcal{L}^n\mathcal{R}}$ with even n. It seems to be impossible to obtain any further results from figure 16. In fact, these seemingly obvious results are wrong.

Firstly we recall (see section 6.3), that the areas $\mathcal{P}_{\mathcal{L}^n\mathcal{R}}$ originate from the two-parametric bifurcation at $B^{\mathrm{II}}(a)$ in the plane $b \times \mu$, which represents for $a > 0$ a period adding big bang bifurcation. Hence, the bifurcation scenario shown in the right part of figure 17(a) cannot be the period increment scenario. In fact, the scenario we observe is the period adding scenario, whereby the bifurcation lines belonging to higher periods lie so close to each other that these periods are difficult to detect. This fact is illustrated in figure 17(c), which is calculated using a sufficiently high sampling rate. As expected, between the parameter intervals belonging to the areas $\mathcal{P}_{\mathcal{L}^{10}\mathcal{R}}$ and $\mathcal{P}_{\mathcal{L}^{12}\mathcal{R}}$, we detect parameter values leading to the orbits $O_{(\mathcal{L}^{10}\mathcal{R})^2\mathcal{L}^{12}\mathcal{R}}$, $O_{\mathcal{L}^{10}\mathcal{R}\mathcal{L}^{12}\mathcal{R}}$ and $O_{\mathcal{L}^{10}\mathcal{R}(\mathcal{L}^{12}\mathcal{R})^2}$.

Next let us compare figure 16 with figures 4, 9 and 10. As one can see, the plane $\mu = 10^{-4}$ is represented in these figures as a horizontal line lying close above the axis $\mu = 0$. Therefore,

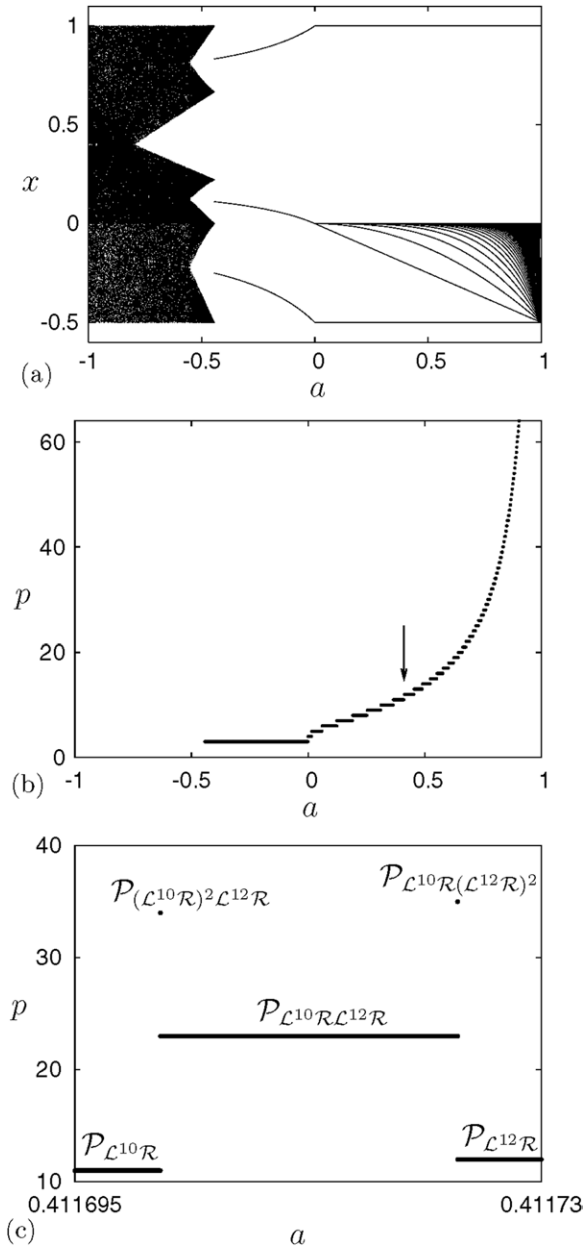

Figure 17. Bifurcation scenario along the line marked in figure 16 ($b = -1.5$, $\mu = 10^{-4}$). The scenario in the right part seems to be a usual period increment scenario, but is in fact the period adding scenario. The arrow in (*b*) marks the tiny interval shown enlarged in (*c*).

for negative values of a the parameter area shown in figure 16 contains the pairwise overlapping regions $\mathcal{P}_{\mathcal{L}\mathcal{R}^{2n}}$ for all n. However, these regions are located very close to the line $b = -1$ and can be observed only by using a very high resolution. Similarly, in the upper part of figure 16 (for $a > 0$) one can observe only periodic behaviour. However, in this figure there is an area with chaotic behaviour as well. This occurs above the intersection of the plane $\mu = 10^{-4}$ with

the surface ξ^{env}. Because the line

$$\xi^{\mathrm{env}}\big|_{\mu=10^{-4}} = a^{\mathrm{env}}(b, 10^{-4}) = \frac{b+1000}{1001} \tag{28}$$

separating the chaotic from the periodic regime lies for $b \in [-2, -1]$ close to the line $a = 1$ (i.e. the boundary of the investigated area $\mathcal{P}$), this fact becomes visible only when using a very high resolution. However, from equation (26) it follows that for any positive value of a there is a sufficiently large negative value of b, so that the behaviour of the investigated system in the plane $\mu = 10^{-4}$ is chaotic for these parameter values.

9. Conclusions

In this paper we have investigated a one-dimensional piecewise linear map with a discontinuous system function, initially introduced in [15]. This map actually represents the normal form of the discrete-time representation of many practical systems in the neighbourhood of the point of discontinuity. We have pointed out that the observed one-parameter bifurcation diagrams showing period increment and period adding scenarios can be properly explained only by pinpointing a few critical points in the 3D parameter space.

In the 2D sections of the parameter space there exist two-parametric (co-dimension two) big bang bifurcation points, where an infinite number of bifurcation curves meet. In piecewise linear maps these curves are caused by border-collision bifurcations. The big bang bifurcation points have specific influence areas, which determine the character of periodic orbits induced by this bifurcation. We described the occurrence of three different types of two-parametric big bang bifurcations, namely the pure period increment big bang bifurcations, the period increment big bang bifurcations with coexistence of attractors and the period adding big bang bifurcations. Depending on these types we explained such phenomena as the occurrence of orbits with progressively higher periodicities in arithmetic progression, with or without overlapping in the parameter space. The cases where higher periodic or chaotic orbits are sandwiched between the ranges of occurrence of consecutive periodic orbits in that progression are expained as well.

Furthermore, we have demonstrated that an infinite number of the two-parametric bifurcations (especially their types and relative positions) is organized by a few three-parametric or co-dimension three bifurcation points in the 3D parameter space. It is shown how several complex bifurcation scenarios and structures, which can be observed under variation of one or two parameters, can be explained taking into account the influence of the three-parametric bifurcations.

A few open problems relating to the dynamics of system (2) investigated in this work still remain. In particular, we stated that the investigated region $\mathcal{P}$ is not completely covered by the areas $\Omega(B^{\mathrm{I}}(0))$, $\Omega(B^{\mathrm{II}}(0))$ and $\mathcal{P}^{\mathrm{ch}}$. Our preliminary investigation shows that there exist some further three-parametric bifurcations in the area $\mathcal{P}$, which have not yet been described in detail.

Additionally, the two-parametric bifurcations occurring at the points $B^{\mathrm{II}}(a)$, which we detected in this work, have to be investigated as well. Another interesting problem concerns the structure of the area $\mathcal{P}^{\mathrm{ch}}$ with chaotic behaviour. We have found that in this area there are some regions leading to one-band chaotic attractors and some other regions leading to multi-band chaotic attractors. There is some evidence indicating that the structure of these areas is strongly influenced by a new class of big bang bifurcation which causes unstable periodic orbits to occur. This type of big bang bifurcation has not been reported until now and represents a great challenge for further work.

References

[1] Banerjee S, Karthik M S, Yuan G H and Yorke J A 2000 Bifurcations in one-dimensional piecewise smooth maps—theory and applications in switching circuits *IEEE Trans. Circuits Syst.—I* **47** 389–94

[2] Banerjee S and Grebogi C 1999 Border collision bifurcations in two-dimensional piecewise smooth maps *Phys. Rev.* E **59** 4052–61

[3] di Bernardo M, Feigin M I, Hogan S J and Homer M E 1999 Local analysis of C-bifurcations in n-dimensional piecewise smooth dynamical systems *Chaos, Solitons Fractals* **10** 1881–908

[4] Yuan G H, Banerjee S, Ott E and Yorke J A 1998 Border collision bifurcations in the buck converter *IEEE Trans. Circuits Systems—I* **45** 707–16

[5] Zhusubaliyev Zh T, Soukhoterin E A, Rudakov V N, Kolokolov Y V and Mosekilde E 2001 Bifurcations and chaotic oscillations in an automatic control relay system with hysteresis *Int. J. Bifurcation Chaos* **11** 1193–231

[6] Nordmark A B 1991 Non-periodic motion caused by grazing incidence in an impact oscillator *J. Sound Vib.* **145** 279–97

[7] Budd C and Dux F 1994 Chattering and related behaviour in impacting oscillators *Phil. Trans. R. Soc.* **347** 365–89

[8] Dankowicz H and Nordmark A B 2000 On the origin and bifurcations of stick–slip oscillations *Physica D* **136** 280–302

[9] Sun J, Amellal F, Glass L and Billette J 1995 Alternans and period-doubling bifurcations in atrioventricular nodal conduction *J. Theor. Biol.* **173** 79–91

[10] Thuilot B, Goswami A and Espiau B 1997 Bifurcation and chaos in a simple passive bipedal gait *Proc. IEEE Int. Conf. on Robotics and Automation (Albuquerque, NM, USA)*

[11] Feely 0 and Chua L 0 1992 Nonlinear dynamics of a class of analog-to-digital converters *Int. J. Bifurcation Chaos* **22** 325–40

[12] Maggio G M, di Bernardo M and Kennedy M P 2000 Nonsmooth bifurcations in a piecewise-linear model of the Colpitts oscillator *IEEE Trans. Circuits Systems—I* 1160–77

[13] Banerjee S, Parui S and Gupta A 2004 Dynamical effects of missed switching in current-mode controlled dc–dc converters *IEEE Trans. Circuits Systems—II* 649–54

[14] Sharkovsky A N and Chua L O 1993 Chaos in some 1-D discontinuous maps that appear in the analysis of electrical circuits *IEEE Trans. Circuits Systems—I* **40** 722–31

[15] Jain P and Banerjee S 2003 Border collision bifurcations in one-dimensional discontinuous maps *Int. J. Bifurcation Chaos* **13** 3341–52

[16] Takens F 1974 Applications of global analysis: forced oscillations and bifurcations *Commun. Math. Inst. Rijksuniversiteit Utrecht* **3** 1–59

[17] Arnold V I 1977 Loss of stability of autooscillations near resonances and versal deformations of equivariant vector fields *Funct. Anal. Appl.* **11** 1–10

[18] Zaks M A, Lyubimov D B and Pikovsky A S Universal scenarios of transitions to chaos via homoclinic bifurcations *Preprint* 192(87) (Sverdlovsk: Russian Academy of Science, Institute of mechanics of solid matter) (in Russian)

[19] Lyubimov D V, Pikovsky A S and Zaks M A 1989 *Universal Scenarios of Transitions to Chaos via Homoclinic Bifurcations* (*Math. Phys. Rev.* vol 8) (London: Harwood Academic)

[20] Ghrist R and Holmes P 1994 Knotting within the gluing bifurcation *Proc. IUTAM Symp. on Nonlinearilty and Chaos in the Enginnering Dynamics* ed J Thompson and S Bishop (New York: Wiley) pp 299–315

[21] Ghrist R 2000 Resonant gluing bifurcations *Int. J. Bifurc. Chaos* **10** 2141–60

[22] Kuznetsov Y 2004 *Elements of Applied Bifurcation Theory* 3rd edn (Berlin: Springer)

[23] Dankowicz H and Zhao X 2005 Local analysis of co-dimension-one and co-dimension-two grazing bifurcations in impact microactuators *Physica* D **202** 238–57

[24] Kowalczyk P and di Bernardo M 2005 Two-parameter degenerate sliding bifurcations in Filippov systems *Physica* D **204** 204–29

[25] Kowalczyk P, di Bernardo M, Champneys A R, Hogan S J, Homer M, Kuznetsov Yu A, Nordmark A and Piiroinen P 2006 Two-parameter nonsmooth bifurcations of limit cycles: classification and open problems *Int. J. Bifurc. Chaos* **16**

[26] Nordmark A and Kowalczyk P 2006 A codimension-two scenario of sliding solutions in grazing–sliding bifurcations *Nonlinearity* **19** 1–26

[27] Kluiving R, Capel H W and Pasmanter R A 1992 Symbolic dynamics of fully developed chaos *Physica* A183

[28] Hao B-L 1991 Symbolic dynamics and characterization of complexity *Physica* D **51** 161–76

[29] Avrutin V, Wackenhut G and Schanz M 1999 On dynamical systems with piecewise defined system functions *Proc. Int. Conf. Tools for Mathematical Modelling MATHTOLS'99 (St Petersburg)* pp 4–20

[30] Avrutin V and Schanz M 2006 On multi-parametric bifurcations in a scalar piecewise-linear map *Nonlinearity* **19** 531–52
[31] Avrutin V and Schanz M 2005 On special types of two- and three-parametric bifurcations in piecewise–smooth dynamical systems *WSEAS Trans. Math.* **4** 224–30
[32] Avrutin V 2004 On behavior of dynamical systems with piecewise-smooth system function *PhD Thesis* University of Stuttgart (in German)
[33] Lagarias J C and Tresser C 1995 A walk along the branches of the extended Farey tree *IBM J. Res. Dev.* **39** 283–94
[34] Chin W, Ott E, Nusse H E and Grebogi C 1994 Grazing bifurcations in impact oscillators *Phys. Rev.* E **50** 4427–44
[35] Casas F, Chin W, Grebogi C and Ott E 1996 Universal grazing bifurcations in impact oscillators *Phys. Rev.* E **53** 134–9
[36] Ganguli A and Banerjee S 2005 Dangerous bifurcation at border collision: when does it occur? *Phys. Rev.* E **71** 057202
[37] Birman J and Williams R F 1983 Knotted periodic orbits in dynamical systems—i: Lorenz's equations *Topology* **22** 47–82
[38] Avrutin V and Schanz M 2005 Border-collision induced bifurcation phenomena and multi-parametric bifurcations in a piecewise-quadratic map on interval *Proc. Conf. on 5th EUROMECH Nonlinear Dynamics 'ENOC 2005' (Eindhoven)*